geologicaacta

*Citation:* Bover-Arnal, T., Pascual-Cebrian, E., Moreno-Bedmar, J.A., Salas, R., 2025. Strontium-isotope stratigraphy of the Aptian–Albian transition in the western Maestrat Basin (E Iberia). Geologica Acta, 23.27, 1-pgs. DOI: 10.1344/GeologicaActa2025.23.27
Online ISSN: 1696-5728



# Strontium-isotope stratigraphy of the Aptian–Albian transition in the western Maestrat Basin (E Iberia)

**Telm Bover-Arnal**[1,2] **Enric Pascual-Cebrian**[1] **Josep Anton Moreno-Bedmar**[3] **Ramon Salas**[1,2]

[1]**Departament de Mineralogia, Petrologia i Geologia Aplicada, Facultat de Ciències de la Terra, Universitat de Barcelona**
c/ Martí i Franquès s/n, 08028 Barcelona, Catalonia, Spain. Bover-Arnal E-mail: telm.boverarnal@ub.edu
Pascual-Cebrian E-mail: enricpascual@hotmail.com Salas E-mail: ramonsalas@ub.edu

[2]**Institut de Recerca GEOMODELS**
c/ Martí i Franquès s/n, 08028 Barcelona, Catalonia, Spain

[3]**Instituto de Geología, Universidad Nacional Autónoma de México**
Ciudad Universitaria, Coyoacán, 04510 Ciudad de México, Mexico. Moreno-Bedmar E-mail: josepamb@geologia.unam.mx

## ABSTRACT

The Aptian–Albian transition in the Maestrat Basin (E Iberian Chain) encompasses two lithostratigraphic units: the Benassal and Escucha formations. In some sectors of the basin, such as the western Galve and Las Parras sub-basins, this stratigraphic interval recorded a progressive shift from widespread carbonate platform settings to coastal siliciclastic-influenced and coal-bearing environments. Due to the transitional nature of this interval, establishing a clear stratigraphic boundary between the upper part of the Benassal Formation and the lower part of the Escucha Formation is challenging. Additionally, there is no unanimous agreement on the age range of these formations. To shed light on the stratigraphic location of the boundary between the Aptian and the Albian, strontium-isotope analyses were carried out on thirteen low-Mg calcite oyster shells to derive numerical ages. In the Las Parras Sub-basin, the $^{87}Sr/^{86}Sr$ values obtained from the siliciclastic-influenced transitional deposits between the Benassal and Escucha formations, as well as from the lowermost part of the Escucha Formation, range from 0.707282±0.000002 to 0.707410±0.000002. These Sr-isotope ratios translate into numerical ages that constrain this stratigraphic interval to the early Albian. The oyster shells collected in the Galve Sub-basin exhibit a higher degree of diagenetic alteration. Nevertheless, the least altered specimens analysed from the lower part of the transitional facies between the Benassal and Escucha formations in this latter sub-basin yielded Sr-isotope ratios between 0.707197±0.000003 and 0.707256±0.000002. These values correspond to ages spanning from the latest Aptian to the earliest Albian. Accordingly, in most sectors of the western Maestrat Basin, the Aptian–Albian boundary is likely to be stratigraphically located at the lowermost part of the transitional facies between the Benassal and Escucha formations.

***KEYWORDS*** **Strontium-isotope stratigraphy. Geochronology. Escucha Formation. Early Cretaceous. Iberian Chain.**

## INTRODUCTION

The Aptian–Albian transition in the Maestrat Basin (Eastern Iberian Chain; Fig. 1) recorded a shift from open marine carbonate platform conditions (*e.g.* Canérot *et al.*, 1982; Salas, 1987), to more coastal environments influenced by siliciclastic deposition and coal formation (*e.g.* Pardo Tirapu, 1979; Querol Carceller, 1990). This stratigraphic interval encompasses two lithostratigraphic units: the Benassal Formation (Canérot *et al.*, 1982) below, and the Escucha Formation (Aguilar *et al.*, 1971) above (Fig. 2). The Benassal Formation is characterized by an alternation of marls and well-bedded to nodular grey limestones, rich in orbitolinids, corals, rudist bivalves, and nerineid gastropods (*e.g.* Bover-Arnal *et al.*, 2014; Martín-Martín *et al.*, 2013). Its upper part recorded a progressive shallowing of the depositional environment and includes skeletal and oolitic limestones with a grainstone texture, sandy limestones, and sandstones that are often ferruginous and frequently display cross-bedding structures, along with

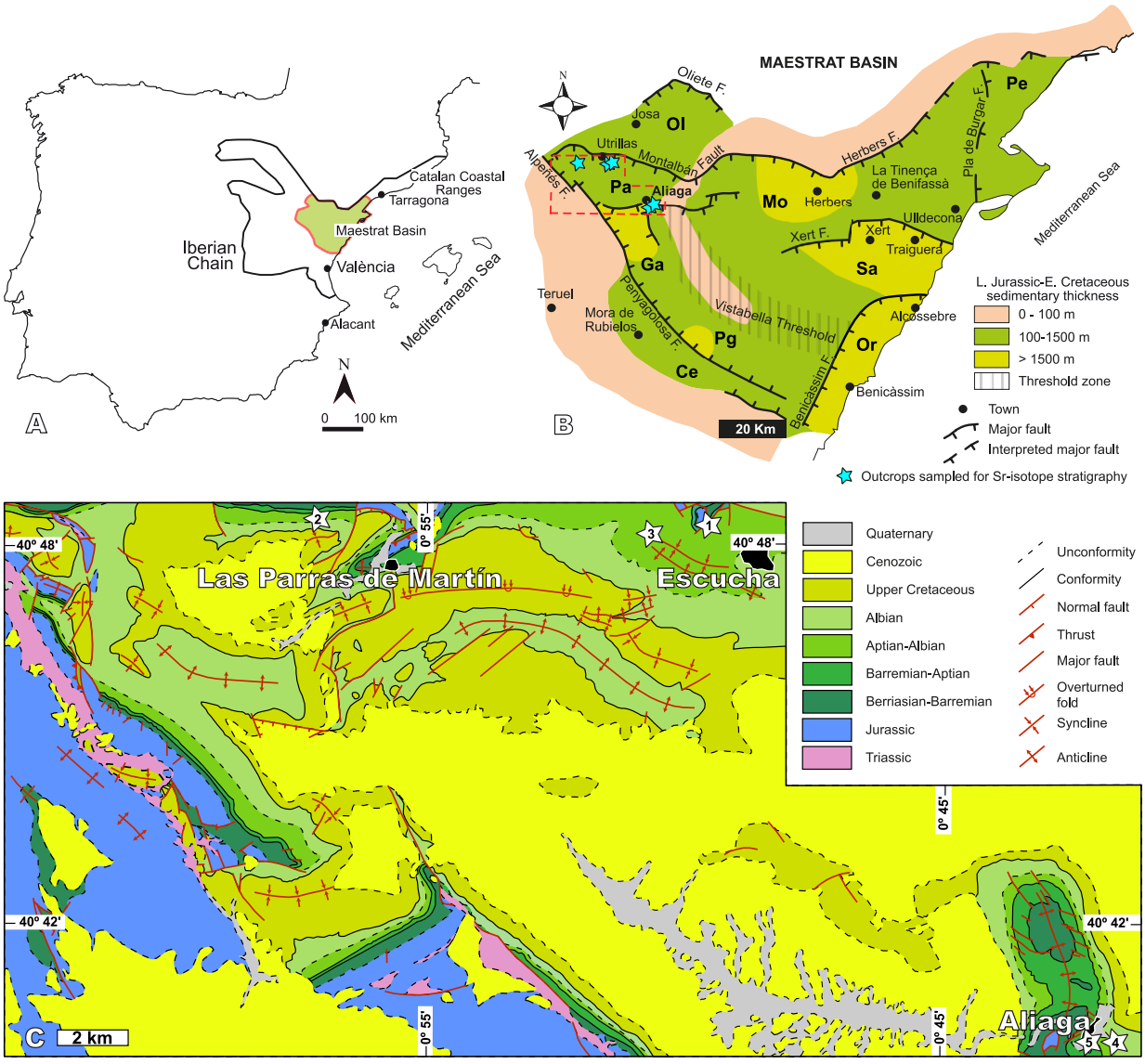


**FIGURE 1.** Geological setting. A) Map of the Iberian Peninsula highlighting the Maestrat Basin, located in the eastern sector of the Iberian Chain. B) Simplified structural and isopach map of the Maestrat Basin during the Late Jurassic–Early Cretaceous. The outcrops sampled for Sr-isotope stratigraphy within the Galve and Las Parras sub-basins are marked with blue stars. The different sub-basins are labeled as follows: Mo (Morella), Pe (El Perelló), Sa (La Salzedella), Ga (Galve), Ol (Oliete), Pa (Las Parras), Ce (Cedramán), Or (Orpesa), and Pg (Penyagolosa). Dashed red line outlines the area covered by the geological map in Figure 1C. This map is adapted from Salas *et al.* in Martín-Chivelet *et al.* (2019). C) Geological map showing the location of the outcrops sampled for Sr-isotope stratigraphy within the Galve and Las Parras sub-basins, modified from Martín Fernández and Canérot (1977) and Canérot *et al.* (1979). The outcrops sampled are indicated with white stars and correspond to: 1) Los Peregrines, 2) Mina Salomé, 3) Cabezo del Moral, 4) Barranco de la Virgen and 5) Las Cubetas.

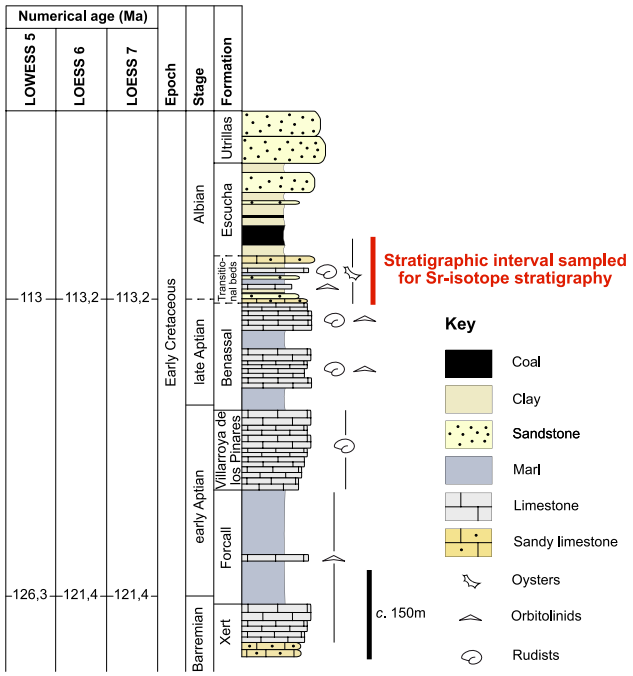


**FIGURE 2.** Synthetic stratigraphic log of the latest Barremian–Albian sedimentary succession in the western Maestrat Basin, showing the stratigraphic interval sampled for Sr-isotope stratigraphy, and the stratigraphic position of the Aptian–Albian boundary as inferred from the results of this study. The numerical ages of the Barremian–Aptian and Aptian–Albian boundaries are taken from the LOWESS/LOESS look-up tables 5, 6 and 7 of McArthur *et al.* (2012), McArthur *et al.* (2020) and McArthur and Howarth (2024), respectively.

marls, and clays that may be partially coaly (Bover-Arnal *et al.*, 2010; Canérot *et al.*, 1982). The lower part of the Escucha Formation consists of alternating beds of marl, clay, coal, sandstone, and bioclastic limestone and sandy limestone (Pardo Tirapu, 1979; Querol Carceller, 1990; Querol *et al.*, 1992; Rodríguez-López *et al.*, 2009).

Accordingly, the facies of the upper part of the Benassal Formation closely resemble those of the lower part of the Escucha Formation. Consequently, where the Escucha Formation overlies the siliciclastic-influenced upper part of the Benassal Formation, its lower boundary is difficult to define due to the absence of a significant sedimentary break (Canérot *et al.*, 1982; Querol Carceller, 1990). This ambiguity in transitional facies can result in the same stratigraphic interval being attributed to either the uppermost Benassal Formation or the lowermost Escucha Formation, depending on the interpretation of individual authors. Lithostratigraphic units such as formations are inherently interpretative. In some cases, such interpretative discrepancies may account for the differing age assignments of the basal part of the Escucha Formation reported in the literature (see *e.g.* Villanueva-Amadoz *et al.*, 2010, for a review of the different age assignments).

This issue was already recognized by the cartographers of the Geological and Mining Institute of Spain (IGME) in the late 1970s, who produced the 1:50,000 geological maps of the area. In these maps (Canérot *et al.*, 1979; Martín Fernández and Canérot, 1977), the Aptian–Albian transition was included within a broad mapping unit encompassing the uppermost part of the Benassal Formation and the Escucha Formation (Fig. 1C), referred to as the 'Transitional Facies' (Canérot *et al.*, 1979).

In contrast, in many sectors of the north-northwestern areas of the basin (Fig. 1B), the base of the Escucha Formation is clearly marked by an unconformity, resting on deposits from the lower Aptian, Barremian, Jurassic, or Triassic (Pardo Tirapu, 1979; Querol Carceller, 1990; Salas *et al.*, 1995). An additional challenge in determining the age of the base of the Escucha Formation is its likely diachronous nature across the basin (*e.g.* Boulouard and Canérot, 1970; Canérot *et al.*, 1982).

In this regard and based on the authors' interpretation of the stratigraphic intervals studied as the Escucha Formation, Boulouard and Canérot (1970) assigned an upper Aptian–Albian age to the Escucha Formation in the Las Parras Sub-basin, while attributing a late Aptian age in the southeastern Morella Sub-basin and a late Albian age in the northeastern La Salzadella Sub-basin (Fig. 1B). Aguilar *et al.* (1971) interpreted the Escucha Formation as late Aptian–Albian in age, based on their analysis of charophyte and ostracod records from the Las Parras and Galve sub-basins (Fig. 1B). In the Oliete Sub-basin (Fig. 1B), Peyrot *et al.* (2007a) studied the miospore and dinoflagellate cyst record from the lower part of the Escucha Formation, dating it to the upper Aptian-lower Albian. Additionally, within the Oliete Sub-basin, de Gea *et al.* (2008) dated the base of the Escucha Formation as upper Aptian based on nannofossils and planktonic foraminifera. On the other hand, Querol and Solé de Porta (1989) and Solé de Porta *et al.* (1994) analysed the palynofacies of the Escucha Formation in the Morella Sub-basin and in the Las Parras and Oliete sub-basins (Fig. 1B), respectively. Their studies assigned a lower to middle Albian age to this lithostratigraphic unit. In line with these latter findings, Martínez *et al.* (1994) and Moreno-Bedmar *et al.* (2008) determined, based on ammonoid findings, that in La Salzedella Sub-basin (Fig. 1B), the lowermost part of the Escucha Formation dates to the lower Albian. In this sub-basin, the lowermost part of the Escucha Formation includes the *Leymeriella tardefurcata* Zone and probably, the lower part of the *Douvilleiceras mammillatum* Zone.

On the other hand, the Benassal Formation was originally dated as upper Aptian–early Albian by Canérot *et al.* (1982). More recently, Martín-Martín *et al.* (2013) also proposed, based on orbitolinid analysis in the Orpesa Sub-basin (Fig. 1B), that the uppermost part of the Benassal

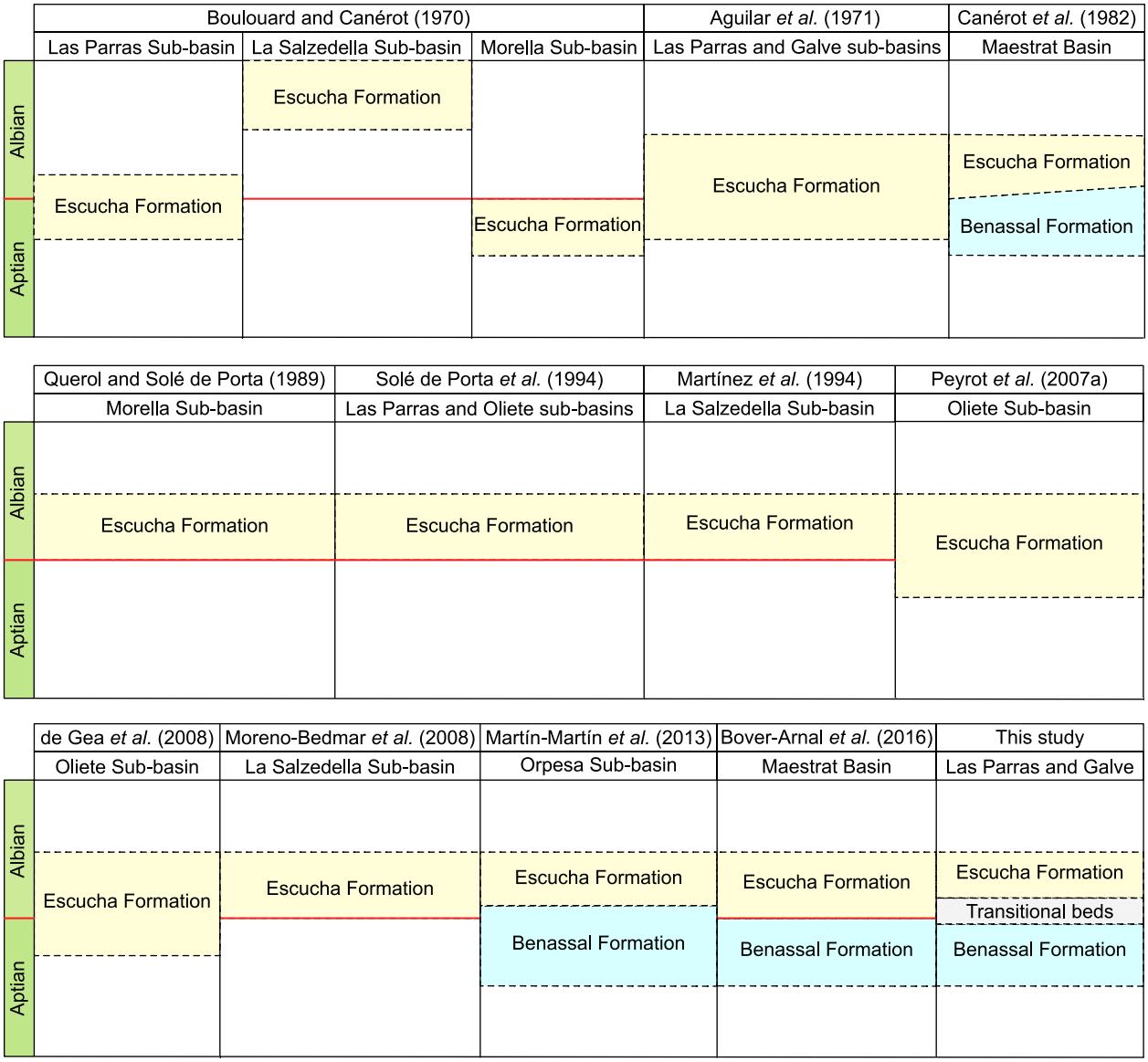


**FIGURE 3.** Summary chart showing the age ranges attributed to the Benassal and Escucha formations in different sub-basins of the Maestrat Basin, as reported in previous studies and refined in the present work.

Formation could extend into the early Albian. Bover-Arnal *et al.* (2016) assigned an age range from the latest early Aptian to the late Aptian for the Benassal Formation and placed the Aptian–Albian boundary at the contact between the Benassal and Escucha formations. Figure 3 presents a summary chart compiling the different ages that have been assigned to the Benassal and Escucha formations by various studies conducted across the different sub-basins of the Maestrat Basin.

Using strontium-isotope stratigraphy performed on oyster shells, this study investigates the age of the transitional interval between the Benassal and Escucha formations in the western Maestrat Basin, specifically in the Galve and Las Parras sub-basins (Fig. 1B). In these sub-basins, the transition between the two lithostratigraphic units is gradual and encompasses the boundary between the Aptian and Albian stages. The results are of relevance, as the lower and middle members of the Escucha Formation, known as Barriada and Regachuelo (Cervera *et al.*, 1976), are rich in coal deposits (*e.g.* Querol *et al.*, 1992), which have been historically exploited in the region. Additionally, these coal beds host amber deposits (*e.g.* Delclòs *et al.*, 2007; Peñalver *et al.*, 2007) that preserve a remarkable diversity of insects (*e.g.* Pérez-de la Fuente *et al.*, 2020) and resinicolous fungal remains (*e.g.*

Speranza *et al.*, 2015). The lower and middle members of the Escucha Formation also contain a rich and diverse palaeofloral assemblage (*e.g.* Peyrot *et al.*, 2007b; Sender *et al.*, 2020; Villanueva-Amadoz *et al.*, 2010). The numerical ages derived from the Sr-isotope analyses provide new insights into the stratigraphic positioning of the Aptian–Albian boundary in the western Maestrat Basin, as well as refining the chronological framework for the formation of these coal and amber deposits, along with their associated palaeobotanical assemblage.

## GEOLOGICAL SETTING

The Maestrat Basin was a Mesozoic extensional basin located in the eastern Iberian Plate (Fig. 1A). It developed as a result of two rifting cycles. The first, occurring from the Kimmeridgian to early Berriasian, was linked to the opening of the North Atlantic, while the second, from the Barremian to early Albian, was associated with the formation of the Bay of Biscay (García-Senz and Salas, 2011; Salas *et al.*, 2010). These tectonic events subdivided the basin into nine distinct sub-basins: Las Parras, Galve, Oliete, Morella, El Perelló, La Salzedella, Penyagolosa, Cedramán, and Orpesa (Salas *et al.* in Martín-Chivelet *et al.*, 2019). Throughout this time, thick accumulations of Upper Jurassic–Lower Cretaceous marine and continental carbonates and siliciclastic sediments were deposited and buried, exceeding 1.5km in depocentral areas (Fig. 1B).

In the western Maestrat Basin (Fig. 1B), the Galve and Las Parras sub-basins contain a marine-to-continental transitional stratigraphic interval, which comprises the upper part of the Benassal Formation and the lower part of the Escucha Formation, both of which are described in the previous section. This interval, which is the focus of the present study, also encompasses the Aptian–Albian boundary (Figs. 1C; 2). During the Alpine orogeny (late Eocene–early Miocene), compressional forces resulting from the collision between the Iberian and Eurasian plates led to the basin's inversion, ultimately shaping the eastern sector of the Iberian Chain (Guimerà, 1994, 2018). This tectonic contraction deformed and exposed the Triassic to Cretaceous sedimentary record in the region (Fig. 1C). Today, these Mesozoic rocks are partially covered by Palaeogene to Neogene conglomerates, sandstones, clays, and locally, lacustrine limestones and marls.

The late Barremian–early Aptian sedimentary succession underlying the Benassal Formation, consists of, from oldest to youngest, the Xert, Forcall and Villarroya de los Pinares formations (Fig. 2). The Xert Formation is composed of marine sandstones and sandy limestones in its lower part, while its middle to upper parts are dominated by marls and limestones containing orbitolinids (Canérot *et al.*, 1982; Salas, 1987), mainly *Palorbitolina lenticularis* (*e.g.* Bover-Arnal *et al.*, 2016). The overlying Forcall Formation (Canérot *et al.*, 1982; Salas, 1987) represents deeper marine facies compared to the Xert Formation (Fig. 2). It consists of alternating marls and limestones rich in large discoidal *Palorbitolina lenticularis*, and ammonoids. This formation has been precisely dated to the terminal Barremian–early Aptian based on ammonite biostratigraphy and includes the four lower Aptian ammonite zones: *Deshayesites oglanlensis*, *Deshayesites forbesi*, *Deshayesites deshayesi*, and *Dufrenoyia furcata* (Bover-Arnal *et al.*, 2010; Garcia *et al.*, 2014). The Villarroya de los Pinares Formation (Fig. 2) consists of platform carbonates characterized by the presence of rudist bivalves and corals (Canérot *et al.*, 1982; Salas, 1987; Vennin and Aurell, 2001). Bover-Arnal *et al.* (2016) mainly constrained this formation to the late early Aptian (within the *Dufrenoyia furcata* Zone), though it locally also includes the upper part of the *Deshayesites deshayesi* Zone. On the other hand, above the Escucha Formation lies the Utrillas Formation (Fig. 2), which is Albian in age (see Garcia *et al.*, 2014; Villanueva-Amadoz *et al.*, 2011) and made up of an alternation of continental variegated sandstones and clays (Canérot *et al.*, 1982; Rodríguez-López *et al.*, 2009).

Finally, regarding the Escucha Formation, it is worth noting that the interpretation of the substrate and isopach maps provided in Salas *et al.* (1995) and Querol *et al.* (1992), respectively, reveals a distinct structural configuration of the Maestrat Basin during this time interval. North of the localities of Aliaga, Herbers, and La Tinença de Benifassà (Fig. 1B), the basin was compartmentalised into four highly subsident depocentres; Estercuel-Ariño, Aliaga-Utrillas, Castellote, and Calanda (Querol, 1990; Querol *et al.*, 1992), each approximately 20-30km wide, accommodating thicknesses of the Escucha Formation exceeding 500m. South of these localities, two larger-scale depocentres, Traiguera and Santa Bàrbara, each 40-50km wide, accumulated thicknesses up to 200m. All depocentres were bounded by structural thresholds and exhibit semigraben geometries characteristic of extensional tectonics, as illustrated in the cross-sections of Querol *et al.* (1992) and Salas *et al.* (1995). The substrate maps from Salas *et al.* (1995) also reveal uplifted semigraben shoulders and varying degrees of erosion of the underlying lithostratigraphic units. In the northern part of the Maestrat Basin, this compartmentalisation into four deeply subsiding sub-basins is a distinctive feature of the early Albian and the Escucha Formation, marking the final phase of the Barremian–early Albian rifting cycle in the Maestrat Basin. The mechanism that triggered the migration of this extensional deformation toward the northwestern margin of the basin during the early Albian is currently unknown.

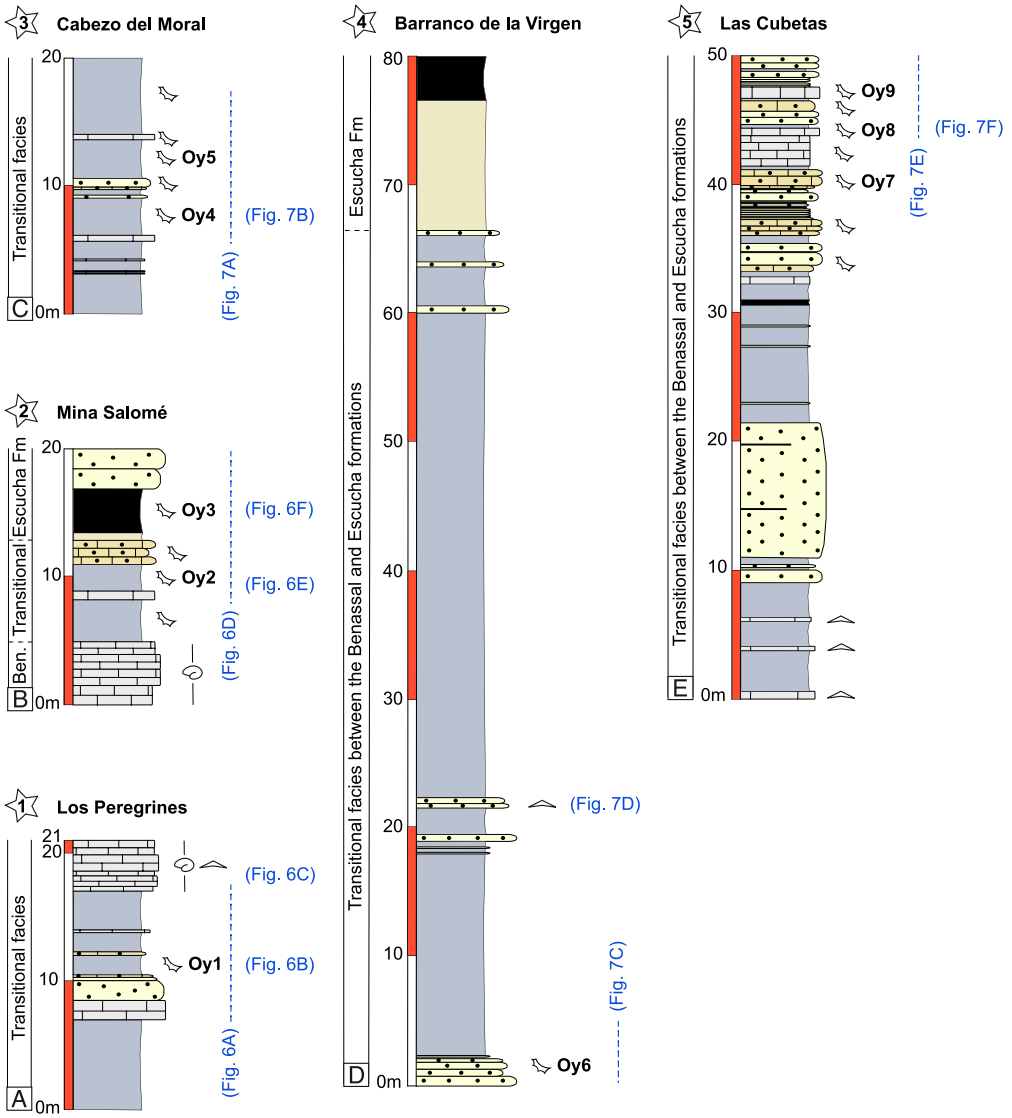


**FIGURE 4.** Stratigraphic logs sampled for Sr-isotope analysis in the western Maestrat Basin. Oy1-9 indicate the stratigraphic situation of the oyster shells collected for this study. The stratigraphic intervals illustrated in Figures 6–7 are also indicated. See Figure 1 for log locations and Figure 2 for the legend. A) Los Peregrines (Las Parras Sub-basin). B) Mina Salomé (Las Parras Sub-basin). C) Cabezo del Moral (Las Parras Sub-basin). D) Barranco de la Virgen (Galve Sub-basin). E) Las Cubetas (Galve Sub-basin).

## MATERIALS AND METHODS

The oyster shells analysed for Sr isotopes were collected from five mixed carbonate-siliciclastic successions spanning the Aptian–Albian transition (Fig. 2), logged in the northern Las Parras and northeastern Galve sub-basins (Fig. 1B). In the Las Parras Sub-basin, the sampled sedimentary successions include Los Peregrines, Mina Salomé, and Cabezo del Moral, while in the Galve Sub-basin, samples were obtained from Barranco de la Virgen and Las Cubetas (Figs. 1C; 4). At Los Peregrines, oysters were sampled from a single stratigraphic interval (Oy1: Lat. 40º 48’ 12.93”N, Long. 0º 49’ 49”W). In Mina Salomé, two oyster banks were analysed (Oy2: Lat. 40º 48’ 19.18”N, Long. 0º 57’ 32.54”W; Oy3: Lat. 40º 48’ 19.10”N, Long. 0º 57’ 32.44”W). At Cabezo del Moral, oysters were collected from two distinct beds (Oy4: Lat. 40º 48’ 05.02”N, Long. 0º 50’ 32.04”W; Oy5: Lat. 40º 48’ 04.83”N, Long. 0º 50’ 31.57”W). A single oyster-bearing level was sampled in Barranco de la Virgen (Oy6: Lat. 40º 40’ 15.54”N, Long. 0º 41’ 48.79”W). At Las Cubetas, oysters were collected from three separate banks (Oy7: Lat. 40º 40’ 13.00”N, Long. 0º 42’ 07.90”W; Oy8: Lat. 40º 40’ 13.78”N, Long. 0º 42’ 07.67”W; Oy9: Lat. 40º 40’ 13.11”N, Long. 0º 42’ 08.14”W). All geographic coordinates are reported in the WGS84 datum, as provided by the FieldMove application

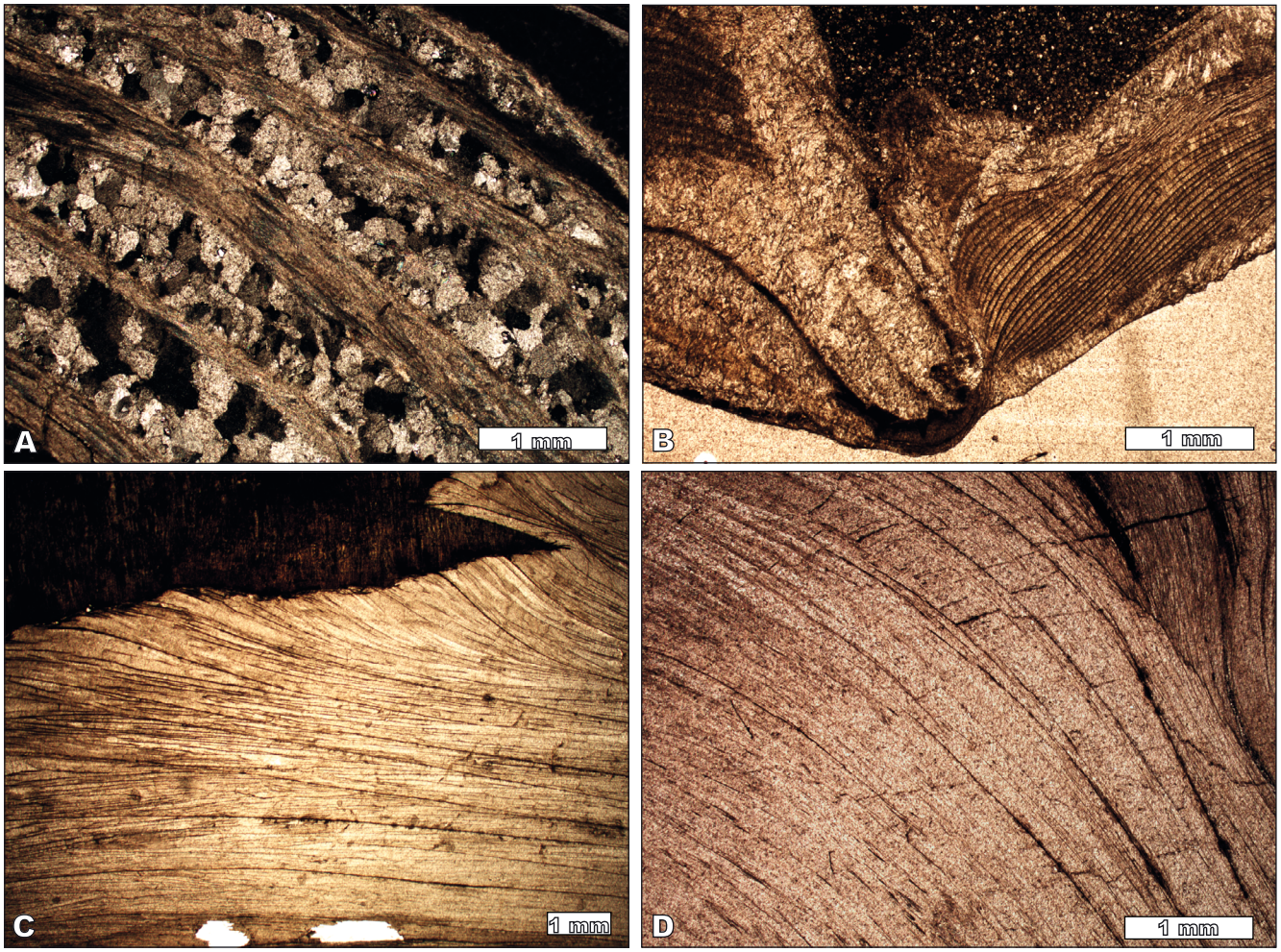


**FIGURE 5.** Diagenetic screening of oyster shells. A) Polarized light photomicrograph of an oyster sample discarded from Sr isotope analysis, showing blocky, equant calcite cements filling structural cavities within the shell. This specimen was sampled from the stratigraphic interval Oy4 at the Cabezo del Moral section (Figs. 1C, 4C). B) Transmitted light photomicrograph of an oyster discarded from Sr isotope analysis, exhibiting extensive recrystallization (left part of the image). The specimen was collected from the stratigraphic interval Oy2 at the Mina Salomé section (Figs. 1C, 4B). C) Transmitted light photomicrograph showing a visually well-preserved oyster shell collected from the stratigraphic horizon Oy7 at the Las Cubetas section (Figs. 1C, 4E). D). Photomicrograph under transmitted light of a visually well-preserved oyster shell retrieved from stratigraphic horizon Oy5 at the Cabezo del Moral section (see Figs. 1C, 4C).

(Petroleum Experts Limited) on an Apple device. In addition, 17 rock samples were collected throughout the five sedimentary successions to produce thin sections for microfacies analysis, providing insights into sedimentary and biotic evolution.

The oyster collection was subjected to diagenetic screening to identify the best-preserved specimens from each sampled stratigraphic interval (Fig. 4). This process followed established methodologies as outlined by several previous studies (*e.g.* Bodin *et al.*, 2009; Boix *et al.*, 2011; Coimbra *et al.*, 2023; Frijia and Parente, 2008; Frijia *et al.*, 2015; Huck *et al.*, 2011; McArthur, 1994; Steuber *et al.*, 2005). In this regard, superficial contamination was removed in an ultrasonic bath filled with deionised water and 5% $H_2O_2$ at 50°C for 5 minutes. Additionally, shells were treated with a 10% HCl solution for 45 seconds, followed by rinsing with deionised water. Subsequently, the shells were examined visually, under a hand lens, and through 27 thin sections prepared for observation under a petrographic microscope, in order to discard those exhibiting cements (Fig. 5A), and/or recrystallized (Fig. 5B), fragmented, or bioeroded areas. The best-preserved valves, showing no significant signs of alteration (Fig. 5C–D), were selected from each of the nine investigated stratigraphic intervals for geochemical analysis. For stratigraphic intervals Oy1 and Oy6–Oy9, one oyster shell was selected per interval, while for intervals Oy2–Oy5, two oyster shells (labelled A and B) were analysed (Table 1).

**TABLE 1.** Analytical results of the low-Mg calcite oyster shells collected within the transitional stratigraphic interval between the Benassal and Escucha formations, around the Aptian–Albian boundary, in the Galve and Las Parras sub-basins of the western Maestrat Basin. NA= Not Applicable. Locality acronyms: LP= Los Peregrines (Las Parras Sub-basin); MS= Mina Salomé (Las Parras Sub-basin); CM= Cabezo del Moral (Las Parras Sub-basin); BV= Barranco de la Virgen (Galve Sub-basin); LC= Las Cubetas (Galve Sub-basin). See Figure 1C for the geographic location of the sections and Figure 4 for the stratigraphic positions of the samples. Numerical ages are based on the LOWESS look-up table 5 from McArthur *et al.* (2012), which is calibrated to the Geological Time Scale 2012 (GTS2012; Gradstein *et al.*, 2012), whereas the LOESS look-up tables 6 and 7 (McArthur, 2020; McArthur and Howarth, 2024) are calibrated to the Geological Time Scale 2020 (GTS2020; Gradstein *et al.*, 2020).

| RAW DATA | | | | | | | | | | | LOWESS 5 (GTS2012) (Aptian–Albian boundary = 113 Ma) | | | LOESS 6 (GTS2020) (Aptian–Albian boundary = 113,2 Ma) | | | LOESS 7 (GTS2020) (Aptian–Albian boundary = 113,2 Ma) | | |
|---|---|---|---|---|---|---|---|---|---|---|---|---|---|---|---|---|---|---|---|
| **Sample** | **Locality** | **Lithostrat. Unit** | **$^{87}Sr/^{86}Sr$** | **2 s.e. (x $10^{-6}$)** | **$^{87}Sr/^{86}Sr$ corrected** | **Mg (ppm)** | **Mn (ppm)** | **Fe (ppm)** | **Sr (ppm)** | **Degree of Alteration** | **min** | **Age (Ma)** | **max** | **min** | **Age (Ma)** | **max** | **min** | **Age (Ma)** | **max** |
| **Oy1** | LP | Transitional beds | 0.707412 | 2.492656 | **0.707410** | 1442.74 | 43.70 | 382.20 | 709.29 | Low | 107.5 | **107.7** | 109.4 | 107.5 | **109.3** | 110.0 | 107.0 | **110.1** | 110.8 |
| **Oy2 (A)** | MS | Transitional beds | 0.707316 | 2.723205 | **0.707314** | 1588.88 | 57.40 | 85.34 | 559.55 | Low | 112.1 | **112.4** | 112.6 | 111.9 | **112.1** | 112.3 | 112.0 | **112.1** | 112.2 |
| **Oy2 (B)** | MS | Transitional beds | 0.707311 | 2.812399 | **0.707309** | 546.42 | 36.30 | 339.77 | 810.67 | Low | 112.2 | **112.5** | 112.7 | 112.0 | **112.2** | 112.3 | 112.0 | **112.1** | 112.2 |
| **Oy3 (A)** | MS | Escucha Fm | 0.707302 | 2.463910 | **0.707300** | 1850.71 | 58.13 | 398.12 | 269.95 | Moderate | 112.4 | **112.7** | 113.0 | 112.2 | **112.3** | 112.4 | 112.1 | **112.2** | 112.3 |
| **Oy3 (B)** | MS | Escucha Fm | 0.707346 | 2.376109 | **0.707344** | 2081.88 | 142.14 | 3781.51 | 642.48 | High | 111.2 | **111.6** | 111.9 | 111.4 | **111.6** | 111.8 | 111.6 | **111.8** | 111.9 |
| **Oy4 (A)** | CM | Transitional beds | 0.707299 | 3.117646 | **0.707297** | 1609.64 | 112.14 | 118.82 | 367.09 | Moderate | 112.5 | **112.8** | 113.0 | 112.2 | **112.3** | 112.5 | 112.1 | **112.3** | 112.4 |
| **Oy4 (B)** | CM | Transitional beds | 0.707311 | 2.552384 | **0.707310** | 1294.07 | 41.45 | 90.91 | 530.58 | Low | 112.2 | **112.5** | 112.7 | 112.0 | **112.2** | 112.3 | 112.0 | **112.1** | 112.2 |
| **Oy5 (A)** | CM | Transitional beds | 0.707283 | 2.642058 | **0.707282** | 1217.50 | 137.04 | 2397.42 | 744.08 | Moderate | 112.8 | **113.1** | 113.3 | 112.4 | **112.5** | 112.6 | 112.3 | **112.4** | 112.5 |
| **Oy5 (B)** | CM | Transitional beds | 0.707308 | 3.088313 | **0.707307** | 2355.35 | 167.10 | 66.49 | 321.25 | Moderate | 112.3 | **112.5** | 112.8 | 112.1 | **112.2** | 112.4 | 112.0 | **112.2** | 112.3 |
| **Oy6** | BV | Transitional beds | 0.707200 | 3.016515 | **0.707197** | 982.97 | 55.58 | 2217.92 | 604.22 | Moderate | 115.4 | **NA** | NA | NA | **114.7** | 114.9 | 114.1 | **115.0** | 115.3 |
| | | | | | | | | | | | | | | 113.2 | **113.4** | 114.4 | 113.5 | **113.8** | NA |
| **Oy7** | LC | Transitional beds | 0.707201 | 2.759832 | **0.707198** | 695.83 | 320.44 | 2004.77 | 648.32 | Moderate | 115.5 | **NA** | NA | NA | **114.7** | 114.9 | 114.8 | **115.0** | 115.8 |
| | | | | | | | | | | | | | | 113.2 | **113.4** | 114.4 | 113.3 | **113.5** | 113.8 |
| **Oy8** | LC | Transitional beds | 0.707259 | 2.656714 | **0.707256** | 819.09 | 268.84 | 2711.68 | 696.33 | Moderate | 113.3 | **113.6** | 113.9 | 112.6 | **112.7** | 112.8 | 112.6 | **112.7** | 112.9 |
| **Oy9** | LC | Transitional beds | 0.707218 | 2.972194 | **0.707215** | 1674.79 | 183.87 | 614.90 | 692.80 | Moderate | 115.6 | **115.8** | 116.0 | 114.9 | **115.1** | 115.2 | 115.3 | **115.5** | 115.8 |
| | | | | | | | | | | | 114.2 | **114.5** | 115.0 | 113.0 | **113.1** | 113.4 | 113.0 | **113.3** | 113.5 |

Sampling was conducted using a microdrill equipped with 0.3 to 0.5mm diameter tungsten drill bits. From each sample, two splits of approximately 100mg of calcite powder were prepared for elemental composition and strontium isotope analyses, respectively. Elemental concentrations (Mg, Mn, Fe, Sr) were analysed using inductively coupled plasma–optical emission spectroscopy (ICP-OES) as an additional diagenetic screening step. This analysis was performed with a PerkinElmer Optima 8300 at the Centres Científics i Tecnològics of the Universitat de Barcelona (CCiTUB). The thirteen oyster shells selected were subsequently classified as exhibiting low, moderate, or high alteration, based on Sr, Mn, and Fe concentrations in their calcitic skeletons. Cut-off summary: Sr >500ppm= low alteration, <500ppm= moderate; Mn <100ppm= low, >100ppm= moderate; Fe <400ppm= low, >400ppm= moderate, >2000ppm= high (see Discussion).

The second split was used to measure Sr isotope ratios ($^{87}Sr/^{86}Sr$) using a TIMS-Phoenix® mass spectrometer housed at the Unidad de Geocronología, CAI de Ciencias de la Tierra y Arqueometría at the Universidad Complutense de Madrid. To account for potential interferences from $^{87}Rb$, appropriate corrections were applied during data processing. The $^{87}Sr/^{86}Sr$ ratios were subsequently normalized to a reference value of 0.1194. Raw measurements were corrected using repeated analyses of the NBS 987 international standard, which yielded mean values of 0.710250±0.000011 (2 standard error, n= 9) for samples Oy1–5 and 0.710251±0.000016 (2 standard error, n= 8) for samples Oy6–9. Absolute ages were calculated from $^{87}Sr/^{86}Sr$ ratios using the Locally Weighted Scatterplot Smoothing (LOWESS)/Local Regression (LOESS) look-up tables 5, 6 and 7, developed by McArthur *et al.* (2012, 2020) and McArthur and Howarth (2024). Table 5 is calibrated to the Geological Time Scale 2012 (GTS2012; Gradstein *et al.*, 2012), while tables 6 and 7 are tied to the Geological Time Scale 2020 (GTS2020; Gradstein *et al.*, 2020). Given that all samples lie near the Aptian–Albian boundary, an interval for which both absolute ages and corresponding $^{87}Sr/^{86}Sr$ ratios have been progressively revised in recent years, using three different LOWESS/LOESS tables helped assess the reliability and consistency of the derived numerical ages.

## RESULTS

### The transitional facies in the Las Parras and Galve sub-basins

Five stratigraphic logs were analysed and sampled with a focus on the transitional beds, which are described and illustrated below. These correspond to sedimentary successions spanning the Aptian–Albian transition in the northwestern Las Parras and Galve sub-basins, including Los Peregrines, Mina Salomé, and Cabezo del Moral in the Las Parras Sub-basin, and Barranco de la Virgen and Las Cubetas in the Galve Sub-basin (Figs. 1B–C; 4).

#### *Los Peregrines*

The Los Peregrines section is 21m thick (Figs. 1C; 4A; 6A). It begins with approximately 7m of marls, followed by a 1.5m thick lacustrine limestone bed with a packstone texture containing charophyte remains. Above this, a 1.5m thick sandstone bed is overlain by a centimetre-thick sandstone bed (Fig. 6A), and a centimetre-thick sandy limestone with a packstone texture rich in *Permocalculus*, gastropods, *Pseudocyclammina*, and peloids. Between metre 10.5 and metre 12, there is a marl interval containing abundant oysters. Oyster sample Oy1 was collected from this interval (Figs. 4A; 5A–B). From metre 12 to metre 17, a cm-thick sandy limestone and a limestone bed alternate with m-thick marl layers. These sandy limestone and limestone beds are rich in peloids, fragments of *Permocalculus*, gastropods, oysters, and echinoids, as well as foraminifera such as miliolids, *Pseudocyclammina*, and other textulariids. The uppermost part of the section is characterized by a 4m thick interval of limestone beds with wackestone to packstone textures, rich in rudist bivalves (including *Toucasia*; Fig. 6A, C), gastropods, fragments of oysters, *Marinella lugeoni*, serpulids, orbitolinids, miliolids, peloids and silt- to fine sand-sized quartz grains.

#### *Mina Salomé*

The Mina Salomé section is 20m thick (Figs. 1C; 4B; 6D). It begins with floatstone to rudstone limestones containing rudist bivalves. This is followed by a 3m-thick marl interval, overlain by a 1m-thick limestone exhibiting a mudstone texture. Between meters 8.5 and 11, another marl interval is present, which contains the oldest oysters sampled at Mina Salomé (Oy2; Figs. 4B; 6D–E). This oyster-bearing marl is overlain by cm-thick coarse sandstone beds rich in oysters. Above, a 4m-thick marl interval rich in coal hosts an accumulation of oysters (Figs. 4B; 6D, F), from which sample Oy3 was collected. The top of the succession is characterized by m-thick white sandstone beds (Fig. 4B).

#### *Cabezo del Moral*

The Cabezo del Moral section is also 20m thick (Figs. 1C; 4C; 7A). It commences with a 5.6m-thick interval of marl deposits interbedded with 5 to 10cm-thick nodular limestones exhibiting a mudstone to wackestone texture, locally containing internal moulds of bivalves. The upper part of this marl interval is bioturbated. This marly succession is followed by a 40cm-thick limestone bed with a packstone texture, containing peloids, silt-sized

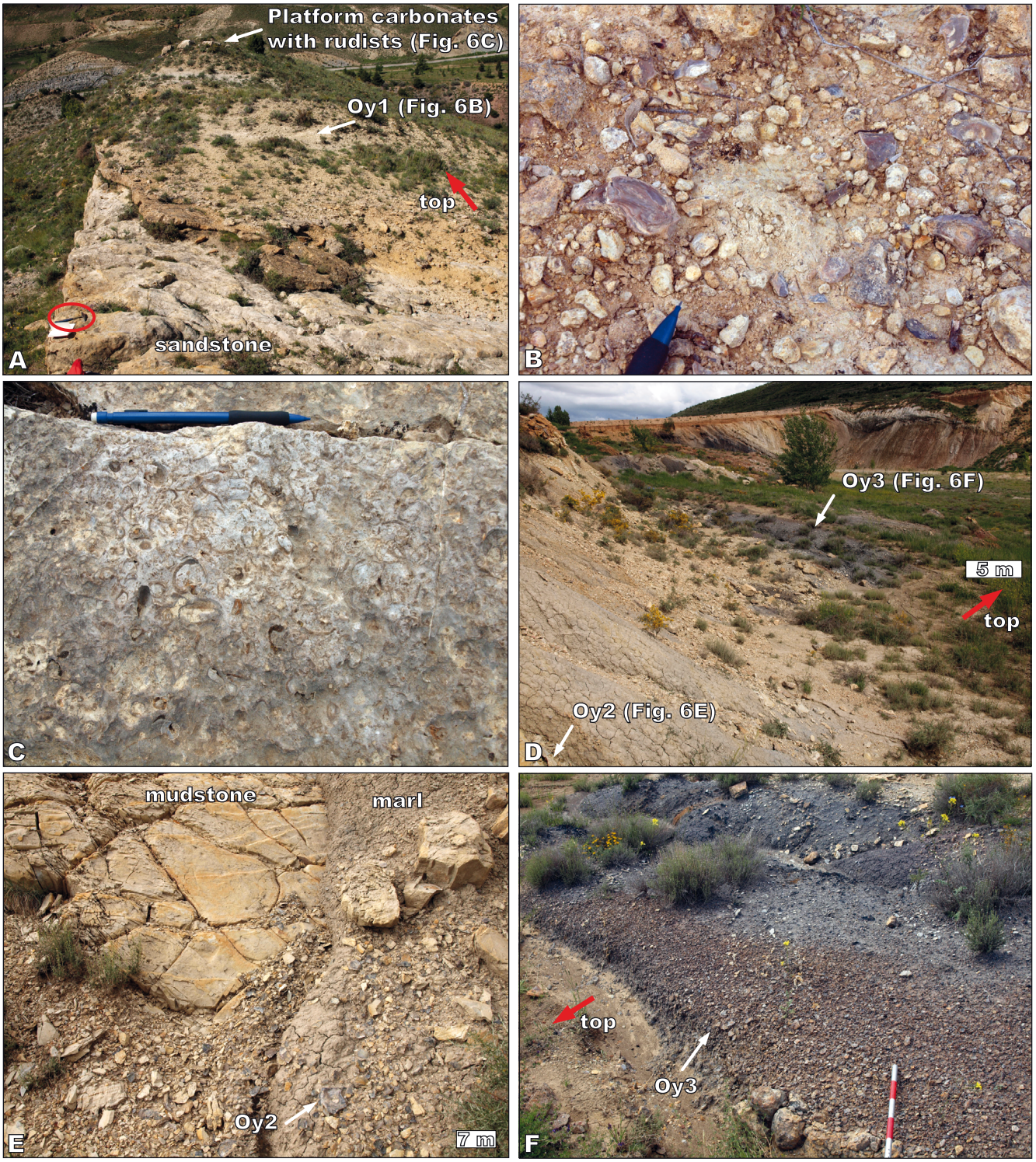


**FIGURE 6.** Los Peregrines and Mina Salomé sections. A) Outcrop view of the Los Peregrines section, showing the marl interval containing oysters sampled for Sr isotope analysis (Oy1), overlain by platform carbonates with rudists. A 32cm-long hammer encircled in red is included for scale. B) Detail of the oyster shells (Oy1) sampled in the Los Peregrines section. Visible part of the pencil= 3.5cm. See Figure 6A for the location of the marl stratigraphic interval containing the oysters collected (Oy1). C) Outcrop photograph of the platform carbonates with rudist bivalves located stratigraphically above the marl interval sampled for oysters (Oy1) in Los Peregrines. Pencil length= 13.8cm. See Figure 6A for the location of these platform carbonates. D) Panoramic view of the upper part of the succession logged at Mina Salomé. E) Detail of the oyster level (Oy2) sampled 4m above the platform carbonates with rudist bivalves of the lower part of the succession logged at Mina Salomé. See Figure 6D for the location of this oyster-bearing level. F) Outcrop photograph of metric-scale coal level containing the oyster accumulation (Oy3) sampled for Sr isotope analysis. Use the visible part of the Jacob's staff for scale; each marked segment of the staff is 10cm. See Figure 6D for the location of the coal-bearing level containing oysters sampled.

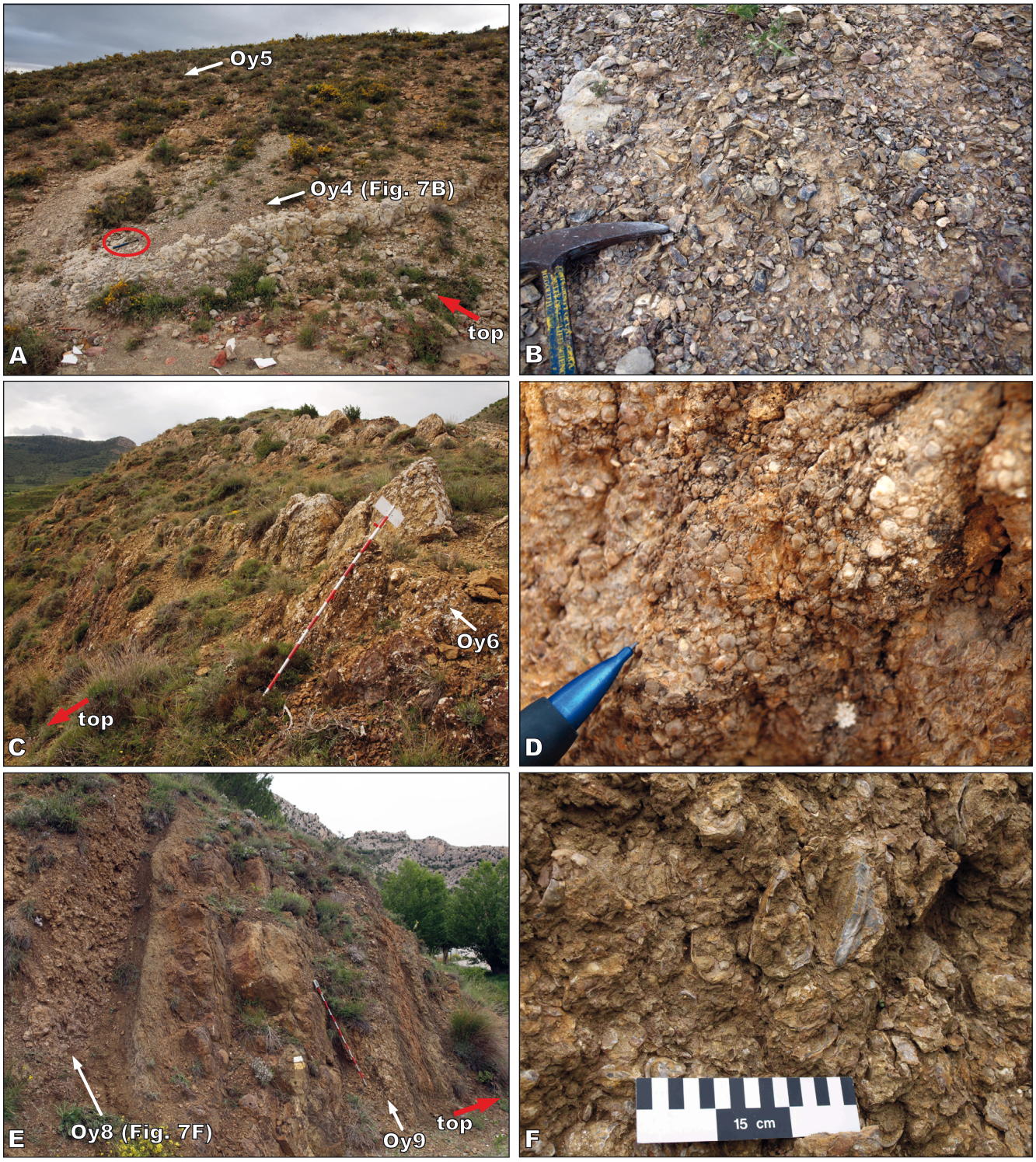


**FIGURE 7.** Cabezo del Moral, Barranco de la Virgen and Las Cubetas sections. A) Outcrop view of the middle and upper parts of the Cabezo del Moral section. Marl beds containing oysters sampled (Oy4 and Oy5) for Sr isotope analysis are indicated. A 32cm-long hammer encircled in red is included for scale. B) Close-up view of Figure 7A showing the oyster level Oy4. Visible part of the hammer= 15cm. C) Outcrop photograph of the lowermost part of the Barranco de la Virgen section indicating the situation of the oysters sampled (Oy6). Jacobs's staff= 1.5m. D) Detail view of the rock-forming orbitolinids occurring in the lower part of the Barranco de la Virgen section. Visible part of the pencil= 3cm. See Figure 4D for the location of these orbitolinid-rich beds. E). Outcrop photograph of the upper part of the Las Cubetas section displaying the stratigraphic location of the oyster beds Oy8 and Oy9 sampled. Jacobs's staff= 1.5m. F) Close-up view of Figure 7E showing the oyster bank (Oy8) sampled at Las Cubetas.

quartz grains, miliolids, textulariids, other foraminifera, and fragments of oysters, other bivalves, gastropods, *Permocalculus*, and echinoids. Above this, there is a 3m-thick marl bed that contains oysters in its lower and middle parts. This oyster-bearing level was sampled as Oy4 (Figs. 4C; 7A–B). The succession continues with a 20cm-thick sandstone, followed by a 50cm-thick marl bed, a 20cm-thick sandy-limestone with fragments of oysters and other bivalves, and an 80cm-thick sandstone. Between metres 10.5 and 13.5, there is a second marl bed rich in oyster shells that was also sampled (Oy5; Figs. 4C; 7A). Above, the succession exhibits a 40cm-thick limestone with a packstone texture containing peloids, silt-sized quartz, miliolids, textulariids, other foraminifera, bivalves, gastropods, *Permocalculus*, echinoids, and sponges. The top of the succession is characterized by a m-thick marl bed with abundant oysters.

### *Barranco de la Virgen*

The Barranco de la Virgen section is 80m thick (Figs. 1C; 4D; 7C). The succession begins with two metres of four cm-thick sandstone beds, showing bioturbation and containing oysters, *Trigonia*, gastropods, and fragments of other skeletal components. Oysters found at the top of the third sandstone bed were sampled as Oy6 (Figs. 4D; 7C). Above this, between metres 2 and 66, the succession is mainly composed of dark marls with a few interbedded cm-thick sandstone layers, which display bioturbation and contain gastropods and *Trigonia*. Between meters 21 and 22, two siliciclastic-influenced beds are present, containing fragments of echinoids, bivalves and gastropods, and orbitolinids in rock-forming abundance (Figs. 4D; 7D). The top of the logged succession consists of a 10m-thick clay layer, overlain by metric coal beds.

### *Las Cubetas*

The Las Cubetas section is 50m thick (Figs. 1C; 4E; 7E). The first 9m of the succession consist of marls interbedded with cm-thick nodular limestones containing orbitolinids in rock-forming abundance. At metre 9, the succession becomes siliciclastic-influenced and is dominated by sandstones up to metre 21. These sandstones exhibit plane-parallel and cross laminations, as well as cross-bedding. Rare mm-thick coal seams also occur

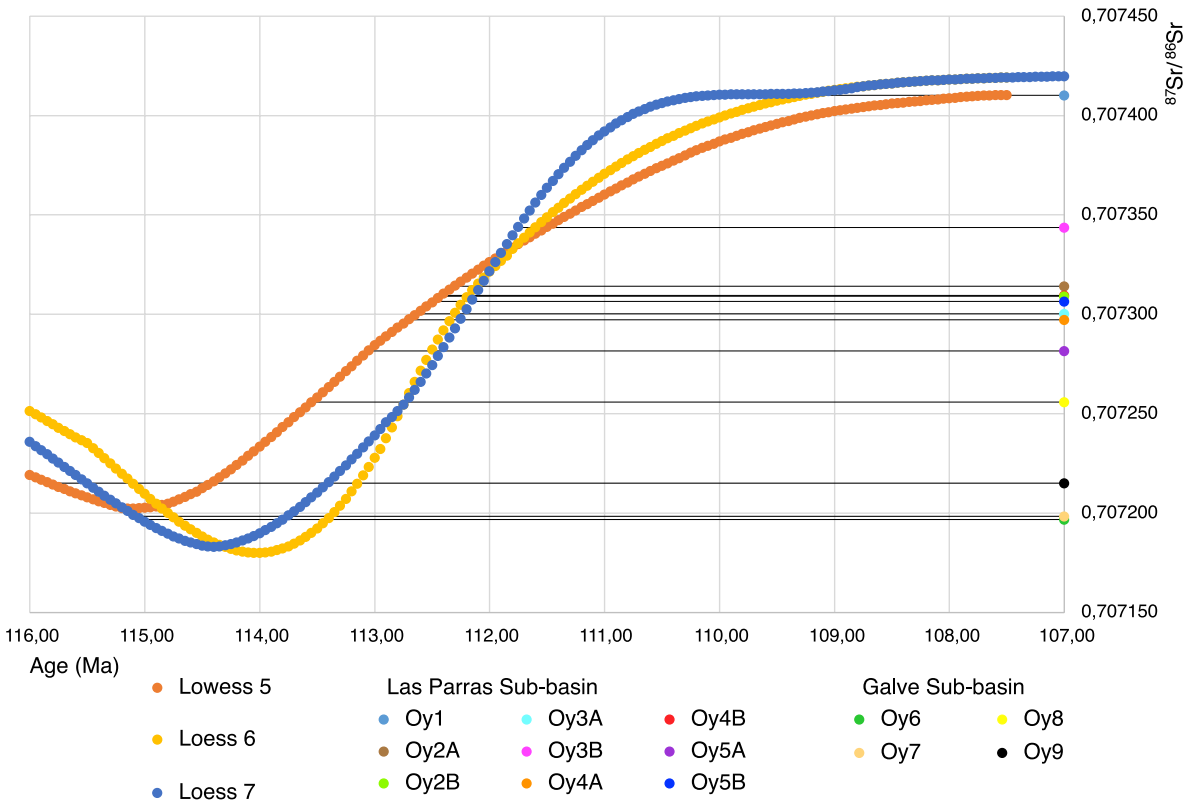


**FIGURE 8.** The graphs show the $^{87}Sr/^{86}Sr$ variations in seawater around the Aptian–Albian boundary for the LOWESS/LOESS look-up tables 5, 6, and 7 of McArthur *et al.* (2012), McArthur *et al.* (2020) and McArthur and Howarth (2024), respectively. The corrected $^{87}Sr/^{86}Sr$ ratios obtained from the samples are plotted, and the intersection between the sample ratios and the curves indicates the corresponding numerical ages, shown on the horizontal axis. The numerical age of the Aptian–Albian boundary is 113Ma and 113.2Ma according to the Geological Time Scale 2012 (Gradstein *et al.*, 2012) and the Geological Time Scale 2020 (Gradstein *et al.*, 2020), respectively.

within the sandstone interval. From metre 21 to metre 33, the succession consists of marls interbedded with cm-thick sandstone beds. At metre 30.3, a 40cm-thick coal layer is present, while at metre 32.6, a 40cm-thick nodular marly limestone with abundant fragmented oysters and other bioclasts occurs. From metre 33 to the top of the logged section, the succession is made up of alternating marls, clays, sandstones, sandy-limestones, and oyster banks (Figs. 4E; 7E–F). The sandstones and sandy limestones are locally bioturbated, and also exhibit plane-parallel and cross lamination, including ripple structures, as well as cross-bedding. The fossil content in the upper part of the succession is dominated by fragmented oyster shells. At metres 40, 44 and 47, three siliciclastic-influenced cm-thick levels with rock-forming oysters accumulations occur and were sampled as Oy7, Oy8, and Oy9, respectively (Figs. 4E; 7E–F). These oyster banks exhibit a rudstone texture and, in addition to oysters, also contain benthic foraminifera and peloids.

## Elemental concentrations (Mg, Mn, Fe, Sr)

The elemental concentrations obtained from the thirteen analysed oysters are detailed in Table 1. The oysters collected from the Las Parras Sub-basin (Oy1–5) show Mg concentrations ranging from 542.42 to 2355.35ppm, while those from the Galve Sub-basin (Oy6–9) exhibit Mg concentrations between 695.83 and 1674.79ppm. The Sr contents in the Las Parras Sub-basin oysters range from 269.95 to 810.67ppm, while in the Galve Sub-basin samples range from 604.22 to 696.33ppm. In the Las Parras Sub-basin, sample Oy4(B) yielded the lowest Mn value of 41.5ppm, whereas the highest value, 142.14ppm, was recorded for Oy3(B). In the Galve Sub-basin, Mn values range from 55.58 (Oy6) to 320.44ppm (Oy7). The Fe record shows a higher disparity of values. While samples Oy1, Oy2, Oy3(A), Oy4, and Oy5(B) from the Las Parras Sub-basin show concentrations ranging from 66.49 to 398.12ppm, samples Oy3(B) and Oy5(A) exhibit notably higher values of 3781.51 and 2397.42ppm, respectively. For the shells collected from the Galve Sub-basin, all samples except Oy9, which yielded an Fe concentration of 614.90ppm, showed values ranging from 2004.77 to 2711.68ppm (samples Oy6–8).

## Sr-isotope ratios and derived numerical ages

The corrected Sr-isotope ratios obtained from the low-Mg calcite oyster shells collected for this study in the Galve Sub-basin (Barranco de la Virgen and Las Cubetas sections) show lower $^{87}Sr/^{86}Sr$ values than those collected from the Las Parras Sub-basin (Los Peregrines, Mina Salomé, and Cabezo del Moral sections) (Table 1). Sample Oy6, collected in the Galve Sub-basin, yielded the lowest $^{87}Sr/^{86}Sr$ value of 0,707197±0.000003, which, according to the LOWESS look-up table 5, translates into a minimum numerical age of 115.4Ma, corresponding to the latest Aptian according to Gradstein *et al.* (2012). Considering the LOESS look-up tables 6 and 7, this Sr-isotope value intersects the seawater $^{87}Sr/^{86}Sr$ variation curves around the Aptian–Albian boundary at two points (Fig. 8). According to LOESS look-up table 6, this value translates into a numerical age of 114.Ma (+0.2) and 113.4Ma (+1/–0.2). Based on Gradstein *et al.* (2020), the older age falls within the latest Aptian, while the younger age spans the latest Aptian to the Aptian–Albian boundary, which is placed at 113.2Ma (Fig. 9). Using the LOESS look-up table 7, the ages obtained are slightly older: 115Ma (+0.3/–0.9) and 113.8Ma (–0.3), both correspond to the latest Aptian (Gradstein *et al.*, 2020).

The Galve Sub-basin samples Oy7 and Oy9, with corrected Sr-isotope values of 0.707198±0.000002 and 0.707215±0.000002, respectively, also intersect the seawater $^{87}Sr/^{86}Sr$ variation curves at two points (Fig. 8). Using the LOWESS look-up table 5, the $^{87}Sr/^{86}Sr$ value for Oy7 translates into a minimum numerical age of 115.5Ma. Considering the LOESS look-up tables 6 and 7, which are tied to Gradstein *et al.* (2020), the Sr-isotope value obtained from sample Oy7 translates into numerical ages of 114.7Ma (+0.2) and 113.4Ma (+1/–0.2), and 115Ma (+0.8/–0.2) and 113.5Ma (+0.3/–0.2), respectively. Following Gradstein *et al.* (2020), all derived ages fall within the latest Aptian, except for 113.2Ma, which marks the Aptian–Albian boundary (Fig. 9). For sample Oy9, the $^{87}Sr/^{86}Sr$ value translates into numerical ages of 115.8Ma (±0.2) and 114.5Ma (+0.5/–0.3), based on the LOWESS look-up table 5 and Gradstein *et al.* (2012). Using the LOESS look-up tables 6 and 7, tied to Gradstein *et al.* (2020), the corrected $^{87}Sr/^{86}Sr$ ratio of sample Oy9 yields ages of 115.1Ma (+0.1/–0.2) and 113.1Ma (+0.3/–0.1), and 115.5Ma (+0.3/–0.2) and 113.3Ma (+0.2/–0.3), respectively. According to the LOWESS look-up table 5, sample Oy9 is dated to the late Aptian. However, when the LOESS look-up tables 6 and 7 are considered, the age ranges derived from the Sr-isotope value of sample Oy9 may extend into the earliest Albian (Fig. 9).

The last low-Mg calcite sample collected in the Galve Sub-basin, Oy8, shows a corrected $^{87}Sr/^{86}Sr$ ratio of 0.707215±0.000002, translating into a preferred latest Aptian numerical age of 113.6Ma (±0.3) according to the LOWESS look-up table 5, which is tied to Gradstein *et al.* (2012). When using the LOESS look-up tables 6 and 7, this Sr-isotope ratio indicates preferred ages of 112.7Ma (±0.1) and 112.7Ma (+0.2/–0.1), respectively. These latter ages would correspond to the earliest Albian according to Gradstein *et al.* (2020).

The corrected $^{87}Sr/^{86}Sr$ ratios measured on oyster shells collected in the Las Parras Sub-basin range between

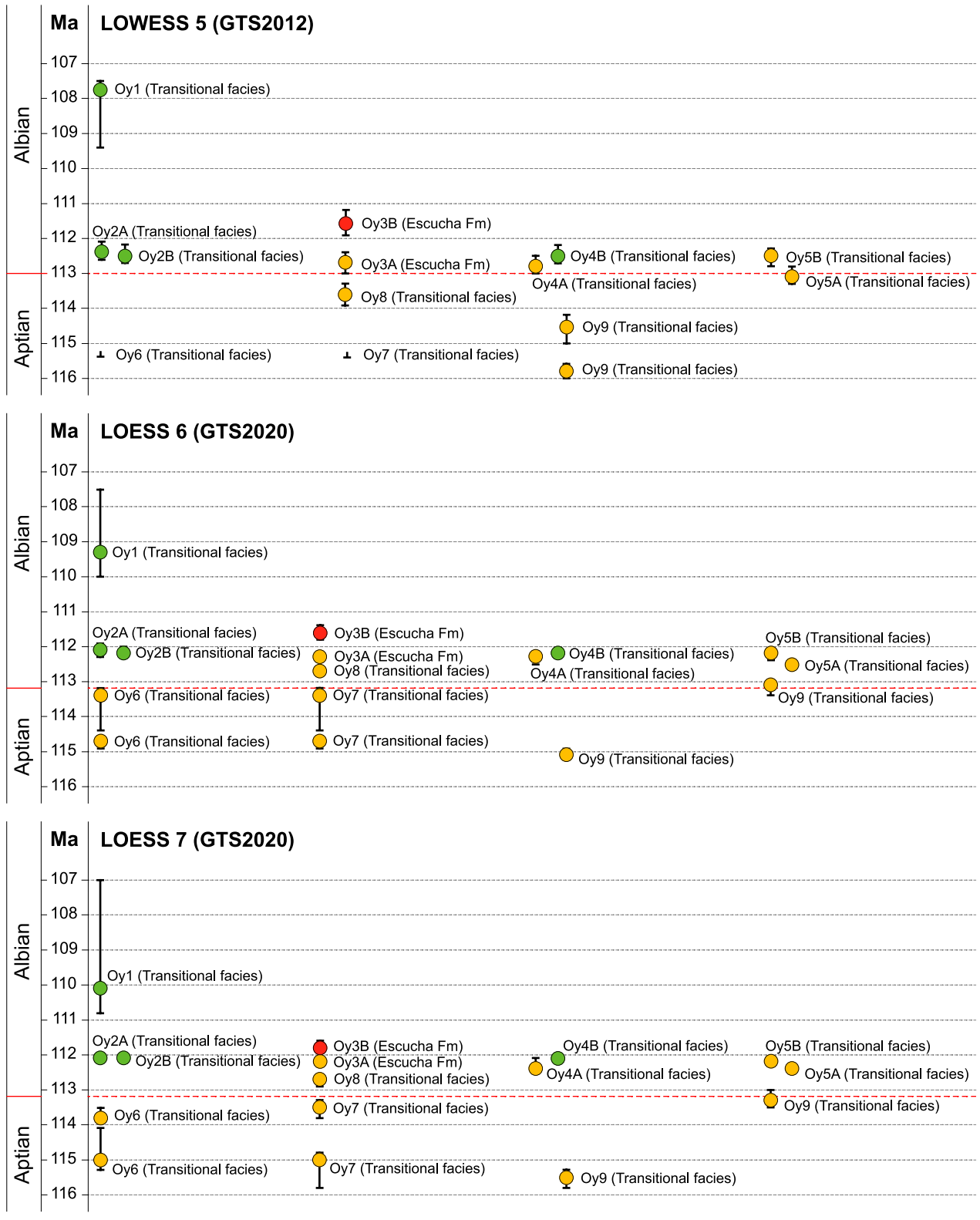


**FIGURE 9.** Numerical ages derived from $^{87}Sr/^{86}Sr$ ratios measured in oyster shells collected from the Escucha Formation and from transitional deposits between the Benassal and Escucha formations, in the Las Parras and Galve sub-basins (western Maestrat Basin). Ages were calculated using the LOWESS 5 and LOESS 6 and 7 look-up tables (McArthur *et al.*, 2012; McArthur, 2020; McArthur and Howarth, 2024), calibrated to the Geological Time Scale 2012 (GTS2012; Gradstein *et al.*, 2012) and the Geological Time Scale 2020 (GTS2020; Gradstein *et al.*, 2020), respectively. Green, orange, and red circles indicate samples with low, moderate, and high degrees of diagenetic alteration, respectively. The distribution of samples along the X-axis is for visualization purposes and does not represent any measured parameter.

0.707282±0.000002 (Oy5A) and 0.707410±0.000002 (Oy1). Using the LOWESS look-up table 5, the Sr-isotope ratio obtained from sample Oy5A translates into a numerical age of 113.1Ma (+0.2/–0.3), which would mainly indicate a latest Aptian age, considering that the Aptian–Albian boundary is located at 113Ma (Gradstein *et al.*, 2012). On the other hand, using the LOESS look-up tables 6 and 7, the preferred ages are 112.5Ma (±0.1) and 112.4Ma (+0.1/–0.1), respectively, placing them in the earliest Albian (Gradstein *et al.*, 2020). Sample Oy5B yielded a corrected $^{87}Sr/^{86}Sr$ ratio of 0.707307±0.000003, which corresponds to numerical ages of 112.5Ma (+0.3/–0.2), 112.2Ma (+0.2/–0.1), and 112.2Ma (+0.1/–0.2), according to LOWESS look-up table 5 and LOESS look-up tables 6 and 7, respectively (Fig. 9). All these absolute age intervals fall within the lower part of the early Albian (Gradstein *et al.*, 2012, 2020).

The two samples collected from the stratigraphic interval Oy4, yielded corrected $^{87}Sr/^{86}Sr$ ratios of 0.707297±0.000003 (Oy4A) and 0.707310±0.000002 (Oy4B). The Sr-isotope ratio of sample Oy4A translates into preferred numerical ages of 112.8Ma (+0.2/–0.3), 112.3Ma (+0.2/–0.1), and 112.3Ma (+0.1/–0.2), according to LOWESS look-up table 5 and LOESS look-up tables 6 and 7, respectively. The $^{87}Sr/^{86}Sr$ value obtained for Oy4B corresponds to ages of 112.5Ma (+0.2/–0.3), 112.2Ma (+0.1/–0.2), and 112.1Ma (±0.1), based on LOWESS look-up table 5 and the LOESS look-up tables 6 and 7, respectively. According to Gradstein *et al.* (2012, 2020), these age intervals fall within the early Albian (Fig. 9).

In the Mina Salomé section, two stratigraphic intervals were sampled (Fig. 4B). The two samples, Oy2A and Oy2B, retrieved from the lower stratigraphic interval, yielded corrected $^{87}Sr/^{86}Sr$ ratios of 0.707314±0.000002 and 0.707309±0.000002, respectively. The $^{87}Sr/^{86}Sr$ value obtained for Oy2A translates into ages of 112.4Ma (+0.2/–0.3), 112.1Ma (±0.2), and 112.1Ma (±0.1), based on LOWESS look-up table 5 and the LOESS look-up tables 6 and 7, respectively. Sample Oy2B derived ages of 112.5Ma (+0.2/–0.3), 112.2Ma (+0.1/–0.2), and 112.1Ma (±0.1), also based on LOWESS look-up table 5 and the LOESS look-up tables 6 and 7, respectively (Fig. 9). Samples Oy3A and Oy3B were collected from the upper part of a metric coal level in Mina Salomé (Figs. 4B; 6F). The corrected $^{87}Sr/^{86}Sr$ ratios obtained for these samples are 0.707300±0.000002 and 0.707344±0.000002, respectively. In accordance with LOWESS look-up table 5 and the LOESS look-up tables 6 and 7, the Sr-isotope ratio of sample Oy3A translates into numerical ages of 112.7Ma (±0.3), 112.3Ma (±0.1), and 112.1Ma (±0.1), respectively, whereas sample Oy3B derived ages of 111.6Ma (+0.3/–0.4), 111.6Ma (±0.2), and 111.8Ma (+0.1/–0.2) (Fig. 9). The numerical ages obtained from the two stratigraphic intervals at the Mina Salomé section indicate an early Albian (Gradstein *et al.*, 2012, 2020).

Finally, sample Oy1 yielded the highest $^{87}Sr/^{86}Sr$ value measured among the collected samples, translating into numerical ages of 107.7Ma (+1.7/–0.2) using the LOWESS look-up table 5, 109.3Ma (+0.7/–1.8) following the LOESS look-up table 6, and 110.1Ma (+0.7/–3.1) according to the LOESS look-up table 7 (Fig. 9). Similar to samples collected at Mina Salomé and Cabezo del Moral, within the same sub-basin, these age intervals also correspond to the early Albian (Gradstein *et al.*, 2012, 2020).

## DISCUSSION

### Lithostratigraphic interpretation

The Benassal Formation is regarded as platform carbonates rich in rudist bivalves, orbitolinids, and *Permocalculus* (*e.g.* Bover-Arnal *et al.*, 2024; Salas, 1987), which gradually transitions towards the Escucha Formation in the western Maestrat Basin, accompanied by a progressive increase in terrigenous material and carbonaceous products (Canérot *et al.*, 1982). The lower member of the Escucha Formation, on the other hand, was described by Canérot *et al.* (1982) as overlying rudist-bearing limestones and consisting of an alternation of clayey or marly layers containing lignite seams, along with sandy limestones and sandstones.

Based on these definitions, the upper part of the Los Peregrines section, which is dominated by platform carbonates rich in rudist bivalves (Fig. 6A, C) and orbitolinids, could be attributed to the Benassal Formation. However, the lower portion of the section, up to metre 17 (Fig. 4A), is made up of alternating marls with oysters, sandy limestones, sandstones, and lacustrine limestones, reflecting continental to transitional conditions. Thus, this succession is more appropriately assigned to the transitional facies. The occurrence of rudist- and orbitolinid-bearing limestones within the transitional facies indicates intervals of reduced terrigenous input, which allowed for the development of carbonate platforms.

On the other hand, the floatstone to rudstone limestones containing rudist bivalves in the lower part of the Mina Salomé section are underlain by more marine, carbonate-rich facies and are thus attributed to the Benassal Formation (Fig. 4B). Above these deposits, a transitional interval is observed in Mina Salomé, consisting of metre-thick marl beds with oysters interbedded with limestones and coarse sandstones, marking a gradual shift from the Benassal to the Escucha Formation. The first metre-thick coal-bearing bed logged at Mina Salomé can be confidently

assigned to the Escucha Formation, representing the onset of characteristic coal-rich facies (Fig. 4B). The Cabezo del Moral succession, in contrast, is entirely interpreted as representing transitional facies with oyster-bearing levels between the Benassal and Escucha formations (Figs. 4C; 7A-B).

In the Barranco de la Virgen and Las Cubetas sections, located in the Galve Sub-basin, the succession displays occasional intercalations of limestones rich in orbitolinids (Figs. 4D; 7D). However, no intercalations of rudist-bearing platform carbonates have been observed. As a result, these successions are interpreted as belonging entirely to the transitional facies between the Benassal and Escucha formations.

These interpretations imply that the lithostratigraphic unit referred to as the 'transitional facies' would be more thickly developed in the Galve Sub-basin than in the Las Parras Sub-basin (Fig. 4), suggesting that the Galve Sub-basin functioned as a more significant depocenter during the Aptian–Albian transition. In contrast, the Las Parras Sub-basin appears to have been a more marginal setting, with a thinner development of transitional deposits (Fig. 4).

Additionally, it is noteworthy that in the central and eastern Maestrat Basin, particularly in the Morella and La Salzedella sub-basins (Fig. 1B), the Escucha Formation exhibits clear transgressive characteristics, evidenced by the presence of ammonites (Bover-Arnal *et al.*, 2016; Martínez *et al.*, 1994; Moreno-Bedmar *et al.*, 2008). In contrast, in the western marginal part of the basin studied, such transgressive indicators are less evident, suggesting that this early Albian transgressive pulse was more localized and restricted to the deeper, more depocentral parts of the basin.

## Evaluation of the reliability of $^{87}Sr/^{86}Sr$ ratios and corresponding numerical ages

The original strontium isotopic composition of marine carbonates, including that of aragonite and calcite shells, can be significantly altered through interaction with diagenetic fluids (*e.g.* Frijia and Parente, 2008; Marcano *et al.*, 2015). In addition to visual inspection of the studied samples using a petrographic microscope (Fig. 5), the assessment of diagenetic alteration in biogenic calcite has traditionally relied on geochemical signatures, particularly the co-occurrence of depleted Sr concentrations with elevated Mn, Fe, and $^{87}Sr/^{86}Sr$ ratios, an association well documented in multicomponent studies (Al-Aasm and Veizer, 1986; Brand *et al.*, 2012; Brand and Veizer, 1980; McArthur, 1994). However, Frijia *et al.* (2015) and Bover-Arnal *et al.* (2016), for example, showed examples where increasing Mn and Fe does not correlate with decreasing Sr concentrations; in those publications high Mn and Fe concentrations were observed in pristine shells with $^{87}Sr/^{86}Sr$ that perfectly matched the seawater composition of the studied intervals. Additionally, other studies have demonstrated that low Mn and Fe concentrations can also reflect diagenetic overprinting (Frijia *et al.*, 2015; Steuber *et al.*, 2005). In this regard, the cut-off values for Mn, Fe, and Sr concentrations used to assess the suitability of samples for strontium-isotope stratigraphy vary among authors (*e.g.* Wierzbowski, 2021). Danise *et al.* (2020) conducted a literature review on the cut-off values used to identify oyster shells that were considered not diagenetically altered. They concluded that such shells typically have Fe and Mn concentrations below 250ppm, and Sr concentrations above 350ppm. However, in deposits directly influenced by freshwater runoff, such as the continental to marine transitional facies studied here (Figs. 2; 4), Fe concentrations up to 700ppm are commonly considered acceptable (*e.g.* Pérez-Cano *et al.*, 2022; Schneider *et al.*, 2009).

Considering these complexities, this study adopts a conservative approach: Mn and Fe concentrations are not employed as primary diagenetic proxies. Instead, visual petrographic assessment combined with Sr concentrations forms the basis for evaluating sample preservation. In this regard, all the analysed samples passed the visual evaluation. Samples with Sr values below 500ppm were considered to show evidence of moderate diagenetic alteration in the current study. Additionally, only oyster shells exhibiting Mn concentrations below 100ppm and Fe concentrations below 400ppm were considered as samples with low alteration and, therefore, their derived numerical ages were deemed reliable (Table 1; Fig. 9).

All samples exhibit $^{87}Sr/^{86}Sr$ ratios consistent with values typical of marine waters during the late Aptian to early Albian (Table 1; McArthur, 2020; McArthur *et al.*, 2012; McArthur and Howarth, 2024). However, only samples Oy1, Oy2A, Oy2B, and Oy4B show values of Sr >500ppm, Fe <400ppm, and Mn <100ppm, and thus are regarded as exhibiting a low degree of alteration (Fig. 9). These samples with low alteration, all collected from the Las Parras Sub-basin (Figs.1B-C; 4A-C), indicate an early Albian age for the stratigraphic intervals sampled within the transitional facies and the Escucha Formation (Table 1).

Samples Oy3A, Oy4A, and Oy5B show Sr concentrations below 500ppm and are therefore interpreted as moderately altered oyster shells, along with Oy5A, which exhibits a Mn concentration above 100ppm and an Fe concentration above 400ppm (Table 1; Fig. 9). However, sample Oy3A, collected within the Escucha Formation about 5m above samples Oy2A-B with low alteration (Figs. 4B; 6D), shows a similar $^{87}Sr/^{86}Sr$ ratio and a slightly older derived numerical age, though still within a comparable age

range to Oy2A-B. Accordingly, the $^{87}Sr/^{86}Sr$ ratio of sample Oy3A is interpreted as not deviating significantly from the original value. Similarly, samples Oy4A and Oy5A-B showing a moderate degree of diagenetic alteration also exhibit $^{87}Sr/^{86}Sr$ ratios and age ranges comparable to relatively well-preserved oyster shell Oy4B (Table 1; Fig. 9). Samples Oy5A-B are stratigraphically located 5m above the oyster shell Oy4B with low alteration (Figs. 4C; 7A). On the other hand, sample Oy3B, exhibiting an Fe concentration of 3781.51ppm and a $^{87}Sr/^{86}Sr$ ratio of 0.707344 (Table 1), significantly different from the ratios measured in samples Oy2A-B and Oy3A, is regarded as having undergone a higher degree of diagenetic alteration (Fig. 9). Therefore, its derived age, which is slightly younger than that of samples Oy2A-B and Oy3A, is considered unreliable.

For the ages derived from the $^{87}Sr/^{86}Sr$ ratios of the samples collected in the Las Parras Sub-basin (Fig. 1B), there is little difference depending on which LOWESS/LOESS look-up table (5, 6, or 7) is used, except for sample Oy5A. When the age of sample Oy5A is derived using LOWESS look-up table 5, the preferred resulting age is latest Aptian, whereas if it is derived using LOESS look-up tables 6 or 7, the entire age range of the sample falls within the early Albian (Table 1; Fig. 9). Given that sample Oy4B, which exhibits low alteration (Table 1; Fig. 9), was dated to the early Albian and lies only about 4.5m below sample Oy5A (Fig. 4C), it can be inferred that Oy5A also belongs to the early Albian. Accordingly, in this case, LOESS look-up tables 6 and 7 provide more reliable results than LOWESS look-up table 5, as expected from the more recent versions of these tables for deriving numerical ages.

Samples Oy6-9, collected within the lower part of the transitional facies in the Galve Sub-basin (Figs. 1B; 4D-E; 7C-F), exhibit Sr concentrations above 600ppm (Table 1) and thus lie above the lower threshold value of 500ppm established in this study. However, samples Oy6–Oy8 show Fe concentrations exceeding 2000ppm, and samples Oy7–Oy9 exhibit Mn concentrations above 100ppm (Table 1), both surpassing the threshold limits of 400ppm and 100ppm, respectively, as defined above. Therefore, all samples from the Galve Sub-basin are interpreted as having been affected by moderate diagenetic alteration, and their derived ages should consequently be treated with caution (Fig. 9).

## Chronostratigraphic implications

Regardless of the version of the LOWESS/LOESS look-up table used to derive numerical ages from the $^{87}Sr/^{86}Sr$ values obtained, samples with a low degree of diagenetic alteration collected in the Las Parras Sub-basin (Oy1, Oy2A-B, and Oy4B) can be confidently assigned to the early Albian (Fig. 9; Table 1). These include oysters retrieved from siliciclastic-influenced transitional facies (Oy2A-B and Oy4B; Figs. 4B-C; 6D-E; 7A-B), as well as oysters collected from a stratigraphic interval made up of alternating siliciclastic-influenced deposits and platform carbonates with rudists (Oy1; Figs. 4A; 6A-C), also assigned to the transitional facies. Oyster samples Oy5B, which shows a moderate degree of diagenetic alternation and was collected stratigraphically above Oy4A-B in the Cabezo del Moral section (Figs. 4C; 6A), also yielded similar preferred early Albian ages to those of the better-preserved oyster shell Oy4B, reinforcing the age determinations obtained for the Las Parras Sub-basin. The same applies to the moderately-altered oyster shells Oy4A and Oy5A. Although the derived ages are slightly older than those obtained for samples Oy4B and Oy5B, the ages calculated using LOESS look-up tables 6 and 7 still fall within the early Albian (Fig. 9). Finally, sample Oy3A, which is also moderately altered, was retrieved from the first coal-bearing level of the Escucha Formation at Mina Salomé (Figs. 4B; 6D, F), located stratigraphically 5 metres above samples Oy2A–B (Figs. 4B; 6D–E). It likewise yielded an early Albian age, with an age range comparable to that of samples Oy2A–B (Fig. 9).

From a lithostratigraphic perspective, and regarding the stratigraphic position of the Aptian–Albian boundary, if the early Albian successions studied in the Las Parras Sub-basin, which comprise platform carbonates with rudist bivalves and orbitolinids alternating with oyster-rich more coastal marls, sandstones, and sandy limestones (Oy1–2; Fig. 6A-E), are assigned to the Benassal Formation, then the Aptian–Albian boundary would lie within the upper part of the Benassal Formation in this sub-basin. Conversely, if these stratigraphic intervals are ascribed to the transitional facies, as done in this study (Oy1–2; Fig. 4A-B), the Aptian–Albian boundary would be situated within the lower part of the transitional facies, or perhaps within the underlying uppermost platform carbonates of the Benassal Formation, but stratigraphically below the metric coal beds of the Escucha Formation (Figs. 2; 9). Accordingly, depending on the depositional environment, characteristic facies of the Benassal Formation, such as limestones with rudists and orbitolinids, may locally be of Albian age in the Las Parras Sub-basin.

The numerical ages derived from the transitional beds of the Galve Sub-basin indicate slightly older ages (Table 1). The four samples collected at the Barranco de la Virgen (Figs. 4D; 7C) and Las Cubetas (Figs. 4F; 7E–F) sections show a moderate degree of diagenetic alteration. Therefore, the numerical ages obtained should be taken with caution. These ages, however, mainly indicate a latest Aptian age, reaching up to the Aptian–Albian boundary when using LOESS look-up tables 6 and 7 tied to Gradstein *et al.* (2020). The exception is sample Oy8 (Figs. 4E; 7E–F),

which, when analysed using LOESS look-up tables 6 and 7 tied to Gradstein *et al.* (2020), yields numerical ages corresponding to the early Albian (Fig. 9). However, this sample exhibits the second-highest Fe and Mn concentrations among all the samples analysed (Table 1), casting doubt on the validity of an early Albian age for the entire transitional facies in the Las Cubetas section.

Among all the samples collected in the Galve Sub-basin (Fig. 1B), sample Oy9 displays the lowest Mn and Fe concentrations, suggesting it is the best-preserved of the group. When analysed using LOESS look-up table 6, the Sr-isotope ratio intersects the curve at two points (Table 1; Fig. 8), one of which yields a preferred age of 113.1 Ma, corresponding to the early Albian according to Gradstein *et al.* (2020) (Fig. 9). However, this early Albian age, derived from a moderately altered sample, is obtained only when using LOESS look-up table 6, making the result uncertain, but not invalidating an early Albian age for the entire transitional facies in the Galve Sub-basin. Based on the available data, the most plausible interpretation is that in the Galve Sub-basin, the boundary between the Aptian and the Albian is located within the lower to middle parts of the siliciclastic-influenced transitional deposits, and thus stratigraphically below the metric coal beds that can be unambiguously assigned to the Escucha Formation (Fig. 2).

Thus, the obtained ages vary depending on the LOWESS/LOESS look-up tables used to derive numerical ages (Figs. 8; 9), the sample location, and the degree of diagenetic alteration of the calcite skeletons analysed (Table 1). Nevertheless, the presented data, which show slight age differences between localities, consistently cluster around the Aptian–Albian boundary (Fig. 9). These minor age variations between localities suggests that the upper boundary of the Benassal Formation, along with the influx of siliciclastic materials into the basin and the establishment of more coastal conditions that characterize the transitional facies, could be slightly diachronous across the western Maestrat Basin. This also applies to the boundary between these transitional facies and the first coal-bearing layers, which are characteristic of the Escucha Formation. In this regard, the diachrony of the Escucha Formation across the Maestrat Basin has already been noted by previous authors (*e.g.* Canérot *et al.*, 1982).

In other sub-basins of the Maestrat Basin where these transitional facies are absent, the stratigraphic position of the Aptian–Albian boundary appears to differ, according to the available literature. In the Orpesa Sub-basin (Fig. 1B), this boundary is located within the Benassal Formation. Preliminary orbitolinid biostratigraphic data reported by Martín-Martín *et al.* (2013) document the presence of *Orbitolina (Conicorbitolina) conica*, suggesting that the uppermost part of the Benassal Formation in this sector is of Albian age (Fig. 3), possibly even late Albian. In contrast, in the Traiguera area, within La Salzedella Sub-basin (Fig. 1B), the lower part of the Escucha Formation contains the complete record of the *Leymeriella tardefurcata* Zone, the first ammonite zone of the early Albian (Garcia *et al.*, 2014; Martínez *et al.*, 1994; Moreno-Bedmar *et al.*, 2008). Consequently, in this locality, the Aptian–Albian boundary would roughly coincide with the base of the Escucha Formation (Bover-Arnal *et al.*, 2016; Fig. 3), suggesting that the stratigraphic hiatus between the Benassal and Escucha formations is minor or even negligible.

## CONCLUSIONS

The aim of the study is not to determine the precise stratigraphic position of the boundary between the Benassal and Escucha formations, but rather to calibrate the transitional stratigraphic interval between these two lithostratigraphic units in the western Maestrat Basin through numerical dating. Based on numerical ages derived from $^{87}Sr/^{86}Sr$ ratios measured in oyster shells from the Las Parras Sub-basin, the last carbonate-platform beds with rudists and orbitolinids, as well as the siliciclastic-influenced transitional facies, located stratigraphically below the coal-bearing levels of the lower part of the Escucha Formation, can already be assigned an early Albian age. In comparison with the Las Parras Sub-basin, the oyster shells from the Galve Sub-basin exhibit poorer preservation, which limits the reliability of the numerical age estimates derived from them. Consequently, the results from the Galve Sub-basin are less conclusive. However, the numerical ages obtained from the best-preserved oyster shells in the Galve Sub-basin indicate a latest Aptian to earliest Albian age for the lower-middle part of the siliciclastic-influenced transitional facies. Consequently, it is likely that the transitional deposits between the Benassal and Escucha formations are, to a large extent, Albian in age in the western part of the Maestrat Basin, including intervals of carbonate platform development bearing rudists and orbitolinids.

These findings are consistent with those reported from more depocentral areas of the Maestrat Basin, where the Benassal and Escucha lithostratigraphic units are more expanded, such as La Salzedella and Orpesa sub-basins. In the La Salzadella Sub-basin, ammonites from the earliest Albian zone occur in the lowermost part of the Escucha Formation, whereas in the Orpesa Sub-basin, the orbitolinid assemblage from the uppermost carbonate platforms of the Benassal Formation most likely indicates an Albian age. Ultimately, in the western Maestrat Basin, the metric coal levels of the Escucha Formation that have been exploited in the recent past and host significant fossiliferous amber deposits can be confidently dated to the early Albian.

## ACKNOWLEDGMENTS

We are grateful to Xavier Querol for sharing with us his expertise on the Escucha Formation and the transitional facies of the western Maestrat Basin dated in this study. We also thank Mar Moragas and an anonymous reviewer for their constructive and helpful corrections and suggestions on the manuscript. We are likewise grateful to the invited editor, Joan Guimerà, for handling the manuscript. The study was funded by the Grup de Recerca Reconegut per la Generalitat de Catalunya 2021 SGR-Cat 00349 "Geologia Sedimentària", and the I + D + i research projects IBERCAFO (PID2024-159218NB-I00) and IBERINSULA (PID2020-113912GB-I00), funded by MCIN/AEI/10.13039/501100011033 and the European Regional Development Fund (ERDF).

## REFERENCES

Aguilar, M.J., Ramírez del Pozo, J., Riba, O., 1971. Algunas precisiones sobre la sedimentación y paleoecología del Cretácico inferior en la zona de Utrillas-Villarroya de los Pinares (Teruel). Estudios Geológicos, 27, 497-512.

Al-Aasm, I., Veizer, J., 1986. Diagenetic stabilization of aragonite and low-Mg calcite; I, Trace elements in rudists. Journal of Sedimentary Research, 56, 138-152.

Bodin, S., Fiet, N., Godet, A., Matera, V., Westermann, S., Clément, A., Janssen, N.M.M., Stille, P., Föllmi, K.B., 2009. Early Cretaceous (late Berriasian to early Aptian) palaeoceanographic change along the northwestern Tethyan margin (Vocontian Trough, southeastern France): $\delta^{13}C$, $\delta^{18}O$ and Sr-isotope belemnite and whole-rock records. Cretaceous Research, 30, 1247-1262.

Boix, C., Frijia, G., Vicedo, V., Bernaus, J.M., Di Lucia, M., Parente, M., Caus, E., 2011. Larger foraminifera distribution and strontium isotope stratigraphy of the La Cova limestones (Coniacian–Santonian, "Serra del Montsec", Pyrenees, NE Spain). Cretaceous Research, 32, 806-822.

Boulouard, C., Canérot, J., 1970. Données nouvelles sur l'Aptien supérieur et l'Albien dans le Bas-Aragón et le Maestrazgo (Espagne). Bulletin du Centre de Recherches Pau-SNPA, 4, 453-463.

Bover-Arnal, T., Moreno-Bedmar, J.A., Salas, R., Skelton, P.W., Bitzer, K., Gili, E., 2010. Sedimentary evolution of an Aptian syn-rift carbonate system (Maestrat Basin, E Spain): effects of accommodation and environmental change. Geologica Acta, 8(3), 249-280.

Bover-Arnal, T., Salas, R., Guimerà, J., Moreno-Bedmar, J.A., 2014. Deep incision in an Aptian carbonate succession indicates major sea-level fall in the Cretaceous. Sedimentology, 61, 1558-1593.

Bover-Arnal, T., Moreno-Bedmar, J.A., Frijia, G., Pascual-Cebrian, E., Salas, R., 2016. Chronostratigraphy of the Barremian-Early Albian of the Maestrat Basin (E Iberian Peninsula): integrating strontium-isotope stratigraphy and ammonoid biostratigraphy. Newsletters on Stratigraphy, 49, 41-68.

Bover-Arnal, T., Guimerà, J., Moreno-Bedmar, J.A., Ferràndez-Cañadell, C., Salas, R., 2024. Aptian major changes in accommodation. New sedimentary evidence from the Maestrat Basin (E Iberia). Sedimentary Geology, 459, 106546.

Brand, U., Veizer, J., 1980. Chemical diagenesis of a multicomponent carbonate system; 1, Trace elements. Journal of Sedimentary Research, 50, 1219-1236.

Brand, U., Jiang, G., Azmy, K., Bishop, J., Montañez, I.P., 2012. Diagenetic evaluation of a Pennsylvanian carbonate succession (Bird Spring Formation, Arrow Canyon, Nevada, U.S.A.) — 1: Brachiopod and whole rock comparison. Chemical Geology, 208-309, 26-39.

Canérot, J., Crespo, A., Navarro, D., 1979. Montalbán, hoja n° 518. Mapa Geológico de España 1:50.000. 2ª Serie. 1ª Edición (in Spanish). Madrid, Servicio de Publicaciones, Ministerio de Industria y Energía, 31pp.

Canérot, J., Cugny, P., Pardo, G., Salas, R., Villena, J., 1982. Ibérica Central-Maestrazgo. In: García, A. (ed.). El Cretácico de España. Madrid, Universidad Complutense de Madrid, 273-344.

Cervera, A., Pardo, G., Villena, J., 1976. Algunas precisiones litoestratigraáficas sobre la Formación "lignitos de Escucha". Tecniterrae, 3(14), 25-33.

Coimbra, R., Cabral, M.C., Azerêdo, A.C., Immenhauser, A., 2024. Constraints on the robustness of oyster geochemical proxy data: application to shallow-water carbonates (Lusitanian Basin, W Portugal). Newsletters on Stratigraphy, 57, 131-152.

Danise, S., Price, G.D., Alberti, M., Holland, S.M., 2020. Isotopic evidence for partial geochemical decoupling between a Jurassic epicontinental sea and the open ocean. Gondwana Research, 82, 97-107.

de Gea, G.A., Rodríguez-López, J.P., Meléndez, N., Soria, A.R., 2008. Bioestratigrafía de la Fm. Escucha a partir del estudio de foraminíferos planctónicos y nanofósiles en el sector de Alcaine, Teruel. Geogaceta, 44, 115-118.

Delclòs, X., Arillo, A., Peñalver, E., Barrón, E., Soriano, C., Valle, R.L.D., Bernárdez, E., Corral, C., Ortuño, V.M., 2007. Fossiliferous amber deposits from the Cretaceous (Albian) of Spain. Comptes Rendus - Palevol, 6, 135-149.

Frijia, G., Parente, M., 2008. Strontium isotope stratigraphy in the upper Cenomanian shallow-water carbonates of the southern Apennines: short-term perturbations of marine $^{87}Sr/^{86}Sr$ during the oceanic anoxic event 2. Palaeogeography, Palaeoclimatology, Palaeoecology, 261, 15-29.

Frijia, G., Parente, M., Di Lucia, M., Mutti, M., 2015. Carbon and strontium isotope stratigraphy of the Upper Cretaceous (Cenomanian-Campanian) shallow-water carbonates of southern Italy: Chronostratigraphic calibration of larger foraminifera biostratigraphy. Cretaceous Research, 53, 110-139.

Garcia, R., Moreno-Bedmar, J.A., Bover-Arnal, T., Company, M., Salas, R., Latil, J.L., Martín- Martín, J.D., Gomez-Rivas, E., Bulot, L.G., Delanoy, G., Martínez, R., Grauges, A., 2014. Lower Cretaceous (Hauterivian–Albian) ammonite biostratigraphy in the Maestrat Basin (E Spain). Journal of Iberian Geology, 40, 99-112.

García-Senz, J., Salas, R., 2011. Sedimentary response to continental rifting in Iberia. In: Bádenas, B., Aurell, M., Alonso-Zarza, A.M. (eds.). Abstracts. 28th IAS Meeting of Sedimentology, Zaragoza (Spain), International Association of Sedimentologists (IAS), 31.

Guimerà, J., 1994. Cenozoic evolution of eastern Iberia: Structural data and dynamic model. Acta Geologica Hispanica, 29(1), 57-66.

Guimerà, J., 2018. Structure of an intraplate fold-and-thrust belt: The Iberian Chain. A synthesis. Geologica Acta, 16(4), 427-438.

Huck, S., Heimhofer, U., Rameil, N., Bodin, S., Immenhauser, A., 2011. Strontium and carbon-isotope chronostratigraphy of Barremian-Aptian shoal-water carbonates: Northern Tethyan platform drowning predates OAE 1a. Earth and Planetary Science Letters, 304, 547-558.

Marcano, M.C., Frank, T.D., Mukasa, S.B., Lohmann, K.C., Taviani, M., 2015. Diagenetic incorporation of Sr into aragonitic bivalve shells: implications for chronostratigraphic and palaeoenvironmental interpretations. The Depositional Record, 1, 38-52.

Martín-Chivelet, J., López-Gómez, J., Aguado, R., Arias, C., Arribas, J., Arribas, M.E., Aurell, M., Bádenas, B., Benito, M.I., Bover-Arnal, T., Casas-Sainz, A., Castro, J.M., Coruña, F., de Gea, G.A., Fornós, J.J., Fregenal-Martínez, M., García-Senz, J., Garófano, D., Gelabert, B., Giménez, J., González-Acebrón, J., Guimerà, J., Liesa, C.L., Mas, R., Meléndez, N., Molina, J.M., Muñoz, J.A., Navarrete, R., Nebot, M., Nieto, L.M., Omodeo-Salé, S., Pedrera, A., Peropadre, C., Quijada, I.E., Quijano, M.L., Reolid, M., Robador, A., Rodríguez-López, J.P., Rodríguez-Perea, A., Rosales, I., Ruiz-Ortiz, P.A., Sàbat, F., Salas, R., Soria, A.R., Suarez-Gonzalez, P., Vilas, L., 2019. The Late Jurassic–Early Cretaceous Rifting. In: Quesada, C., Oliveira, J.T. (eds.). The Geology of Iberia: A Geodynamic Approach. Volume 3: The Alpine Cycle. Heidelberg, Springer, 60-63. DOI: https://doi.org/10.1007/978-3-030-11295-0

Martín Fernández, M., Canérot, J., 1977. Argente, hoja n° 517. Mapa Geológico de España 1:50.000. 2ª Serie. 1ª Edición (in Spanish). Madrid, Servicio de Publicaciones, Ministerio de Industria y Energía, 23pp.

Martínez, R., Grauges, A., Salas, R., 1994. Distribución de los ammonites del Cretácico inferior de la Cordillera Costera Catalana e Ibérica Oriental. Cuadernos de Geología Ibérica, 18, 337-354.

McArthur, J.M., 1994. Recent trends in strontium isotope stratigraphy. Terra Nova, 6, 331-358.

McArthur, J.M., Howarth, R.J., 2024. Strontium isotope stratigraphy of the Cretaceous, 24pp. In: Hart, M.B., Batenburg, S.J., Huber, B.T., Price, G.D., Thibault, N., Wagreich, M., Walaszczyk, I. (eds.). Cretaceous project 200 Volume 1: the Cretaceous World. London, The Geological Society, 544 (Special Publications), pp. DOI: https://doi.org/10.1144/SP544-2023-85

McArthur, J.M., Howarth, R.J., Shields, G.A., 2012. Strontium isotope stratigraphy. The Geologic Time Scale, 127-144. DOI: https://doi.org/10.1016/B978-0-444-59425-9.00007-X

McArthur, J.M., Howarth, R.J., Shields, G.A., Zhou, Y., 2020. Strontium isotope stratigraphy, Chapter 7, 211-238. In: Gradstein, F.M., Ogg, J.G., Schmitz, M.D., Ogg, G.M. (eds.). A Geologic Time Scale. Elsevier B.V., 1, 1357pp.

Moreno-Bedmar, J.A., Bulot, L., Latil, J.L., Martínez, R., Ferrer, O., Bover-Arnal, T., Salas, R., 2008. Precisiones sobre la edad de la base de la Fm. Escucha, mediante ammonoideos, en la subcuenca de la Salzedella, Cuenca del Maestrat (E Cordillera Ibérica). Geo-Temas, 10, 1269-1272.

Pardo Tirapu, G., 1979. Estratigrafía y sedimentología de las formaciones detríticas del Cretácico inferior terminal en el Bajo Aragón Turolense. PhD Thesis. Zaragoza, Universidad de Zaragoza, 473pp.

Peñalver, E., Delclòs, X., Soriano, C., 2007. A new rich amber outcrop with palaeobiological inclusions in the Lower Cretaceous of Spain. Cretaceous Research, 28, 791-802.

Pérez-Cano, J., Bover-Arnal, T., Martín-Closas., 2022. Baremian–early Aptian charophyte biostratigraphy revisited. Newsletters on Stratigraphy, 55, 199-230.

Pérez de la Fuente, R., Engel, M.S., Delclòs, X., Peñalver, E., 2020. Straight-jawed lacewing larvae (Neuroptera) from Lower Cretaceous Spanish amber, with an account on the known amber diversity of neuropterid immatures. Cretaceous Research, 106, 104200.

Peyrot, D., Rodríguez-López, J.P., Barrón, E., Meléndez, N., 2007a. Palynology and biostratigraphy of the Escucha Formation in the Early Cretaceous Oliete sub-basin, Teruel, Spain. Revista Española de Micropaleontología, 39, 135-154.

Peyrot, D., Rodríguez-López, J.P., Lassaletta, L., Meléndez, N., Barrón, E., 2007b. Contributions to the palaeoenvironmental knowledge of the Escucha Formation in the Lower Cretaceous Oliete Sub-basin, Teruel, Spain. Comptes Rendus Palevol, 6, 469-481.

Querol Carceller, X., 1990. Distribución de materia mineral y azufre en los carbones de la Foramción Escucha. Relación con los factores geológicos, sedimentológicos y diagenéticos. PhD Thesis. Barcelona, Universitat de Barcelona, 533pp.

Querol, X., Solé de Porta, N., 1989. Precisiones cronoestratigráficas sobre la Fm. Escucha en el sector noroeste de la cuenca del Maestrazgo. Cordillera Ibérica oriental. Acta Geologica Hispanica, 24(2), 73-82.

Querol, X., Salas, R., Pardo, G., Ardevol, L., 1992. Albian coal-bearing deposits of the Iberian Range in northeastern Spain. In: McCabe, J.P., Parrish, J.T. (eds.). Controls on the distribution and quality of Cretaceous Coals. Geological Society of America, 267 (Special Paper), 193-208.

Rodríguez-López, J.P., Meléndez, N., Soria, A.R., de Boer, P.L., 2009. Reinterpretación estratigráfica y sedimentológica de las formaciones Escucha y Utrillas de la Cordillera Ibérica. Revista de la Sociedad Geológica de España, 22, 163-219.

Salas, R., 1987. El Malm i el Cretaci inferior entre el Massís de Garraf i la Serra d'Espadà. Anàlisi de Conca. PhD Thesis. Barcelona, Universitat de Barcelona, 541pp. Website: http://hdl.handle.net/10803/669675

Salas, R., Martín-Closas, C., Querol, X., Guimerà, J., Roca, E., 1995. Evolución tectonosedimentaria de las cuencas del Maestrazgo y Aliaga-Penyagolosa durante el Cretácico inferior. In: Salas, R., Martín-Closas, C. (eds.). El Cretácico inferior del nordeste de Iberia. Publicacions de la Universitat de Barcelona, 13-94.

Salas, R., García-Senz, J., Guimerà, J., Bover-Arnal, T., 2010. Opening of the Atlantic and development of the Iberian intraplate rift basins during the late Jurassic-early Cretaceous. In: Pena dos Reis, R., Pimentel, N. (eds.). Rediscovering the Atlantic: New Ideas for an old sea. Lisbon 2010, II Central & north Atlantic conjugate margins conference, Extended abstracts, volume 3, 245-248. ISBN: 978-989-96923-1-2.

Schneider, S., Fürsich, F.T., Werner, W., 2009. Sr-isotope stratigraphy of the Upper Jurassic of central Portugal (Lusitanian Basin) based on oyster shells. International Journal of Earth Sciences, 98, 1949-1970.

Sender, L.M., Doyle, J.A., Upchurch Jr., G.R., Endress, P.K., Villanueva-Amadoz, U., Diez, J.B., 2020. Evidence on vegetative and inflorescence morphology of Chloranthaceae (Angiospermae) from the Early Cretaceous (middle–late Albian) of Spain. Journal of Systematic Palaeontology, 18, 2015-2042.

Solé de Porta, N., Querol, X., Cabanes, R., Salas, R., 1994. Nuevas aportaciones a la palinología y paleoclimatología de la Formación Escucha (Albiense inferior-medio) en las Cubetas de Utrillas y Oliete. Cordillera Ibérica Oriental. Cuadernos de Geología Ibérica, 18, 203-215.

Speranza, M., Ascaso, C., Delclòs, X., Peñalver, E., 2015. Cretaceous mycelia preserving fungal polysaccharides: taphonomic and paleoecological potential of microorganisms preserved in fossil resins. Geologica Acta, 13(4), 363-385.

Steuber, T., Korbar, T., Jelaska, V., Gusic, I., 2005. Strontium isotope stratigraphy of Upper Cretaceous platform carbonates of the island of Brac (Adriatic Sea, Croatia): implications for global correlation of platform evolution and biostratigraphy. Cretaceous Research, 26, 741-756.

Vennin, E., Aurell, M., 2001. Stratigraphie sequentielle de l'Aptien du sous-basin de Galvé (Province de Teruel, NE de l'Espagne). Bulletin de la Société Géologique de France, 172, 397-410.

Villanueva-Amadoz, U., Pons, D., Diez, J.B., Ferrer, J., Sender, L.M., 2010. Angiosperm pollen grains of Sant Just site (Escucha Formation) from the Albian of the Iberian Range (north-eastern Spain). Review of Palaeobotany and Palynology, 162, 362-381.

Villanueva-Amadoz, U., Sender, L.M., Diez, J.B., Ferrer, J., Pons, D., 2011. Palynological studies of the boundary marls unit (Albian-Cenomanian) from northeastern Spain. Review of Palaeobotany and Palynology, 162, 362-381.

Wierzbowski, H., 2021. Advances and challenges in palaeoenvironmental studies based on oxygen isotope composition of skeletal carbonates and phosphates. Geosciences, 11, 419.

**Manuscript received June 2025;**
**revision accepted September 2025;**
**published Online December 2025.**